

Worcester Polytechnic Institute Digital WPI

Major Qualifying Projects (All Years)

Major Qualifying Projects

April 2011

Automated Processing of Magnetospheric Poynting Flux As Measured by the Fast Auroral SnapshoT Explorer

James Curtis Rehberger
Worcester Polytechnic Institute

Megan L. Van Welie
Worcester Polytechnic Institute

Steven Chen
Worcester Polytechnic Institute

Follow this and additional works at: <https://digitalcommons.wpi.edu/mqp-all>

Repository Citation

Rehberger, J. C., Van Welie, M. L., & Chen, S. (2011). *Automated Processing of Magnetospheric Poynting Flux As Measured by the Fast Auroral SnapshoT Explorer*. Retrieved from <https://digitalcommons.wpi.edu/mqp-all/3261>

This Unrestricted is brought to you for free and open access by the Major Qualifying Projects at Digital WPI. It has been accepted for inclusion in Major Qualifying Projects (All Years) by an authorized administrator of Digital WPI. For more information, please contact digitalwpi@wpi.edu.



MAJOR QUALIFYING PROJECT

SPONSORED BY: SRI INTERNATIONAL

Automated Processing of Magnetospheric Poynting Flux As Measured by the Fast Auroral SnapshoT Explorer

Authors:

Steven CHEN

James REHBERGER

Megan VAN WELIE

On-site Advisors:

Hasan BAHCIVAN

Russell COSGROVE

WPI Advisors:

Professor Andrew KLEIN

Professor David FINKEL

Abstract

This project aims to create automated analytical and visual tools that will aid researchers in studying phenomena occurring in Earth's thermosphere. The study of these phenomena, known collectively as space weather, is of growing importance due to the adverse impacts they have on manned space flight and communication systems. Using data recorded by the Fast Auroral SnapshoT satellite, binned statistical models of the average downward Poynting flux were created, assisting in the further study of space weather's effects on Earth.

Contents

Abstract	i
Executive Summary	vi
Acknowledgments	ix
1 Introduction	1
2 Background	5
2.1 Earth’s Atmosphere	5
2.2 Space Weather and its Effects on Earth	8
2.3 Fast Auroral SnapshoT (FAST) Satellite	10
2.4 Accessing FAST Satellite Data	12
2.5 Coordinate Systems Represented by the FAST Data	16
2.6 Poynting and Kinetic Energy Flux	20
2.7 Geophysical Parameters	23
3 Methodology and Implementation	25
3.1 Automate the Processing of Poynting and Kinetic Energy Flux	26
3.1.1 Export and Preprocess Raw FAST Satellite Data	28
3.1.2 Unify the Preprocessed FAST Satellite Data	31
3.1.3 Calculate the Missing Electric Field Component	40
3.1.4 Optimize and Automate the 2010 MATLAB Routines to Calculate the Poynting and Kinetic Energy Flux	46
3.1.5 Verify the Calculated Poynting Flux	48
3.2 Develop Binned Statistical Visual Models	49

<i>CONTENTS</i>	iii
3.2.1 3D Polar Plots	49
4 Results	51
5 Recommendations	54
6 Conclusion	55
A Algorithms and Calculations	57
A.1 Outlier Removal Algorithm	57
A.2 Poynting Flux Calculations	58
B Authorship and Deliverables	62
B.1 Authorship	62
B.2 Deliverables	63
C Tutorials	66
C.1 SDT and IDL	66
C.2 MATLAB Code	74

List of Figures

2.1	Earth's Ionosphere	6
2.2	Earth's Magnetosphere	7
2.3	Auroral Acceleration Region	8
2.4	Ionospheric Phenomena	9
2.5	FAST Instruments	11
2.6	SDT Software Design	13
2.7	Conceptual View of CDF Files	15
2.8	Geocentric Equatorial Inertial Coordinate System	17
2.9	Equatorial Coordinate System	18
2.10	Data Coordinate System 2	19
2.11	Geocentric Coordinate System	20
2.12	Poynting and Kinetic Energy Flux Observed by a Rocket	21
2.13	Poynting Vector and Magnetic Field Lines	22
2.14	Kp index and ap index	24
3.1	Top Level Block Diagram	25
3.2	Goal 1 Block Diagram	26
3.3	Goal 1 Block Diagram, Step 1	28
3.4	Network Data Facility	29
3.5	SDT Raw Data	30
3.6	Goal 1 Block Diagram, Step 2	32
3.7	Example of Outlier Removal	34
3.8	Example of Histogram	35
3.9	Example of Time Range and Resolution Unification of Data Types	40
3.10	Goal 1 Block Diagram, Step 3	41

3.11	Generated Electric Current	42
3.12	Observed Generated Electric Current Offset	44
3.13	Noise Floor Level for Orbits 3000-3600: Approximately 3 mV/m	45
3.14	Noise Floor Level for Orbits 4000-5000: Approximately 8 mV/m	46
3.15	Goal 1 Block Diagram, Step 4	47
3.16	Goal 1 Block Diagram, Step 5	48
3.17	Goal 2 Block Diagram	49
4.1	Average Poynting Flux in the Northern Hemisphere	51
4.2	Contributing Crossings to the Average Poynting Flux in the Northern Hemisphere	52
4.3	Verification of Calculated Average Poynting Flux	53

Executive Summary

This project was the second iteration of a four year research endeavor proposed by SRI International and funded by the National Science Foundation (NSF). The purpose of this project was to automate the process of calculating and developing binned statistical visual models of the average downward Poynting and kinetic energy flux as recorded by the Fast Auroral SnapshoT (FAST) satellite. These models will ultimately serve to further the understanding of the Sun's energy input into Earth's thermosphere.

Space weather, or any phenomenon that occurs in near-Earth space as a result of the solar wind emitted from Earth's Sun, can have many effects on the Earth including producing the aurora, causing radio and television interferences, creating hazards to orbiting astronauts and spacecrafts, and even triggering power grid failures; it is therefore important to have an accurate space weather prediction system, which will account for these effects. The objective by the end of the fourth year of this project is to produce general circulation models that will attempt to model the global temperature, circulation, and density of Earth's thermosphere. Doing so will further the accuracy of space weather prediction [1].

Continuing on the progress made by the 2010 Worcester Polytechnic Institute (WPI) Major Qualifying Project (MQP), this project (2011) sought to develop Interactive Data Language and MATLAB functions, which enable the production of average downward Poynting and kinetic energy flux models over a given range of orbital data collected by the FAST satellite. This MQP worked to accomplish two main goals:

1. Automate the Poynting and kinetic energy flux processing of the FAST satellite data.
2. Develop binned statistical visual models (i.e. polar plots) of the Poynting flux and kinetic energy flux data recorded by the FAST satellite.

Researchers at the University of California, Berkeley had already preprocessed raw data measured by the FAST satellite and made it available for general use by the public. However, in 2010

communication with Dr. Robert Strangeway of the University of California, Los Angeles revealed that while the preprocessed positional data was correct, the electric and magnetic field data was unreliable due to errors in calculation. Therefore, to accomplish the first goal of this project and correctly calculate the average Poynting and kinetic energy flux, the raw FAST satellite data had to be accessed and re-preprocessed. Using the Satellite Data Tool (SDT), a software suite that enables fast, real-time access to data collected by various satellites, the raw FAST data was successfully downloaded from remote servers maintained by UC Berkeley. Using updated Interactive Data Language routines originally developed by researchers at UC Berkeley and UCLA, the FAST data was re-preprocessed and exported into Common Data Format (CDF) files. Using the original preprocessed positional data as a basis for comparison, the exported data was verified to be correct; however, further verification on the accuracy of the re-preprocessed magnetic and electric field data requires investigation.

Working under the assumption that the magnetic and electric field data were re-preprocessed correctly, 20,000 satellite orbits worth of data were preprocessed and exported using the SDT and IDL routines. Data exported from SDT was separated into six CDF files per orbit: positional, magnetic field, electric field, spin-axis, electron, and ion data. These six data types exported from SDT were represented in various coordinate systems, resolutions, and were recorded over varying time periods. Therefore, unification of the coordinate systems, resolutions, and time ranges of all data in each orbit was completed in MATLAB to allow for the accurate representation of the final Poynting and kinetic energy flux calculations.

Due to a malfunctioning electric field sensor, the FAST satellite was unable to record electric field data along its spin axis. In addition, the electric field data recorded along the magnetic field was deemed unusable due to an excess amount of noise within the signal. By creating and analyzing binned models of the noisy electric field data plotted against the calculated angle between the magnetic field and the projection of the magnetic field onto the satellite's spin plane, a noise floor level was deduced. Theoretically, by limiting the electric field data recorded along the magnetic field to only those values which fell above the noise floor level, recovery of the unrecorded component was feasible through use of trigonometric functions. However, by creating several binned models of the electric field data it was observed that for different ranges of orbits the noise floor level appeared to change. Lacking an efficient method to determine the correct noise floor level for each

orbit, the Poynting and kinetic energy flux was calculated with the electric field components along the magnetic field and the satellite's spin axis set to zero.

Continuing on the progress made by the 2010 MQP, MATLAB routines were developed that enabled automatic calculation of the Poynting and kinetic energy flux for a given range of FAST satellite data. These routines, which were optimized to efficiently work with nearly 20,000 orbits worth of valid FAST data, automatically preprocess and unify the FAST data before completing the Poynting and kinetic energy flux calculations. Using these routines, a database of Poynting and kinetic energy flux for all valid orbits of FAST data can be created.

The data calculated in completion of the first goal of this project was used to create visual binned statistical models that will aid in analyzing the data recorded by the FAST satellite and complete the overall objective of this project. Two independent functions were developed to create these models: "histograms" and "3D polar plots". The histograms function creates binned bar graphs, which provide a means to observe outliers that occur in the electric and magnetic field data recorded by the FAST satellite. By determining and removing outlier data, the Poynting and kinetic energy flux calculations will become more reliable. The 3D polar plots function creates polar plots, which display the final calculated average intensities of the Poynting and kinetic energy flux over a given range of orbits, magnetic local time, magnetic latitude, altitude, and *ap* index (a planetary index for measuring the strength of a disturbance in the Earth's magnetic field [2]). As previously stated, these models will ultimately serve to further the understanding of the Sun's energy input into Earth's thermosphere.

In the final two years of this project, different WPI MQP groups will work towards developing analytical models based on spherical harmonics, which will be used to develop physical interpretations and estimates of the spatial spectrum of the fluxes [1].

Acknowledgments

This project would not have been possible without the aid and support of many talented individuals both inside and out of the SRI and WPI communities.

Firstly, we would like to thank SRI International for sponsoring this project. More specifically, we would like to give our gratitude to Dr. Russell Cosgrove and Dr. Hasan Bahcivan, who proposed this project and provided guidance and support throughout its completion.

We would also like to thank Jack Verneti from the Science Operation Center at University of California, Berkeley for answering our questions about the Satellite Data Tool, and Dr. Robert Strangeway from University of California, Los Angeles for providing support on verifying the various data types we exported from the Satellite Data Tool.

In addition, we would like to thank Mary McCreedy and Carol Leger from SRI International for their help on programming with Interactive Data Language (IDL) and obtaining data from the Sondrestrom radar.

A special thank you also goes out to Hal Huntley for his essential role in setting up the three servers that we used to complete the exportation and preprocessing of the 20,000 orbits of FAST satellite data.

Finally, we would like to thank our project advisor Professor Andrew Klein for his guidance throughout the entirety of the project. His advice and feedback throughout the project motivated us to produce the best product possible.

Chapter 1

Introduction

Space weather, which collectively describes phenomena that occur within near-Earth space, has become an increasingly popular field of study due to the adverse effects it has on Earth. Space weather is mainly caused by the interaction between solar winds, or streams of charged particles emitted by the Sun, and Earth's atmosphere. This interaction can have many effects such as: causing power grid failures, interfering with radio communications, exposing people traveling in high altitude spacecrafts to radiation, and even creating the colors of the aurora. This project aims to model the Sun's energy input into the Earth's thermosphere, quantified by observing the downward Poynting and kinetic energy flux along the Earth's magnetic field lines, so that such space weather phenomena can be correctly characterized. Such characterization can lead to further improvements in the accuracy of ground and air navigation systems, design of manned spacecrafts to reduce radiation exposure, and radio communication systems.

Previous models, which have attempted to quantify the thermosphere have been insufficient due to their basis on probabilistic calculations of "electric field variability", which prevents the use of electric field models for quantification [1]. These calculations are in no way sufficient for real-world interpretations because they neglect the influence of wave heating. As a consequence of using probabilistic models the calculated Poynting and kinetic energy flux are at best approximations of the actual value. Currently the computation of the atmospheric heating rate uses electric potential (ϕ_m), ionospheric Pedersen conductance (Σ_{Pm}), and precipitating particle energy-flux (Φ_m) as inputs; however, these parameters are for ideal situations and accordingly introduce large biases when used in the previous, insufficient models [1]. This project will attempt to rectify this problem by fitting a model directly to the thermosphere from data gathered by the Fast Auroral SnapshoT satellite.

Over the four years of the project, groups from Worcester Polytechnic Institute (WPI) completing their Major Qualifying Projects (MQP) at SRI International will develop analytical models, which will aid in the quantification of the Sun's energy input into the thermosphere. This research will work to further the understanding of space weather prediction, the global temperature, circulation, and density of the Earth's thermosphere [1]. It will also explore the energy conversion from electromagnetic energy to particle kinetic energy that takes place in the auroral acceleration region (AAR) of Earth's atmosphere which creates the aurora [1].

The first year of this project (2010) was completed by two WPI students who worked with SRI researchers Dr. Russell Cosgrove and Dr. Hasan Bahcivan to create a groundwork for calculating the Poynting and kinetic energy flux for a limited number of FAST satellite orbits [1]. Their main goal was to inspect individual samples of preprocessed FAST data for quality and validity, and to apply necessary algorithms to correctly calculate the Poynting and kinetic energy flux for those valid samples [1]. The final product of the 2010 MQP was a series of MATLAB routines, which they used to manually process the Poynting and kinetic energy flux for individual FAST satellite orbits.

The second year of this project (2011) involved three new WPI student researchers working with Dr. Cosgrove and Dr. Bahcivan to create a framework for downloading, preprocessing, quality screening, and calculating the Poynting and kinetic energy flux for all FAST satellite orbits up to January 1, 2000 [1]. Continuing off of the work completed by the 2010 MQP, the 2011 MQP group optimized the MATLAB routines to efficiently process and calculate the Poynting and kinetic energy flux for large batches of FAST satellite orbits [1]. The final product of the 2011 MQP was the creation of MATLAB functions, which automatically created a binned statistical model of the average Poynting and kinetic energy flux over a specified number of FAST satellite orbits.

The third year of this project (2012) will involve three new WPI student researchers. Using tools developed by the previous two years, they will—with the help of SRI advisors—replace the binned statistical model created by the 2011 MQP group with an analytical model of the Poynting and kinetic energy flux based on spherical harmonics [1].

The fourth and final year of this project (2013) will be completed by SRI researchers Dr. Russell Cosgrove and Dr. Hasan Bahcivan and may include WPI students if it is deemed necessary [1]. The SRI researchers will compile all information and observations obtained throughout the

previous three years of the project to develop physical interpretations of the Sun's energy input into Earth's thermosphere [1].

The final goal of this four-year project will be to create analytical models of both the Poynting and kinetic energy flux incident on the atmosphere from data collected by the FAST satellite to aid in the development of an improved quantification of the Earth's thermosphere [1]. These models are needed to drive general circulation models (GCMs), which are physics-based space weather models that attempt to describe the global temperature, circulation, and density of the thermosphere [1]. The two proposed models are in space and spatial frequency. The space frequency models involve spatial maps of the average energy input, for particular values of the model parameters [1]. The spatial-domain models will provide energy input as a function of scale size (in two dimensions) for particular values of the model parameters, which will result in a greatly improved specification over electric potential models on the energy input from the solar winds [1].

This project was proposed by SRI International and funded by the National Science Foundation (NSF). The sponsor of this project, SRI International, is an internationally recognized nonprofit research and development firm. Although its main headquarters are located in the heart of Silicon Valley in the City of Menlo Park, California, SRI International employs a staff of over 1,700 employees worldwide, with facilities branching across the United States and internationally, including offices in Tokyo, Taiwan, and Korea [3]. SRI International conducts client-sponsored research and development for numerous organizations including government agencies, commercial businesses, and various foundations. Through the years, SRI has had a long history of innovating technologies in its various focus areas, which include communications and networks, computing, engineering systems, materials and structures, and robotics. The engineering and systems division of the company focuses on conducting research and development in areas such as sensing, signals and electronic intelligence, wireless communications, and ionospheric and space research. This project falls within the engineering and systems division of the company and was completed at SRI International's main headquarters in Silicon Valley.

This report chronicles the methods and results completed during the second year of the four year project. Continuing the progress made by the 2010 WPI MQP, this project (2011) sought to develop Interactive Data Language and MATLAB functions, which enabled the production of average downward Poynting and kinetic energy flux models over a given range of orbital data

collected by the FAST satellite. This MQP worked to accomplish two main goals:

1. Automate the Poynting and kinetic energy flux processing of the FAST satellite data.
2. Develop binned statistical visual models (i.e. polar plots) of the Poynting flux and kinetic energy flux data recorded by the FAST satellite.

Communication with Dr. Robert Strangeway of the University of California, Los Angeles revealed that the preprocessed FAST satellite data provided by the University of California, Berkeley was processed incorrectly; however, Dr. Strangeway also disclosed that new processing routines have been created that address this issue. Therefore, the first goal of this project involved using the Satellite Data Tool (SDT), created by researchers at UC Berkeley, and new Interactive Data Language (IDL) routines to re-preprocess and prepare all valid (recorded before January 1, 2000) FAST satellite data for further calculation of the Poynting and kinetic energy flux in MATLAB.

Working off of the results calculated in the first goal, the second goal of this project was to create binned statistical visual models of the average Poynting and kinetic energy flux of data collected by the FAST satellite. These models will aid in the effort to characterize the heating of the atmosphere caused by auroral processes, which is an important input parameter for modeling the temperature, density, and circulation of the upper thermosphere. The final two years of the project will work towards the completion of the remaining goals set by the NSF proposal.

Chapter 2

Background

To provide context for the discussion of this project, background information on the atmosphere, space weather, Fast Auroral SnapshoT (FAST) satellite, and the data collected by the FAST satellite is provided. Additionally, procedures for the calculation of Poynting and kinetic energy flux are discussed.

2.1 Earth's Atmosphere

Earth's atmosphere, which consists mainly of nitrogen and oxygen molecules with many other trace elements, is divided into five main layers. Listed from the lowest to highest elevations, these five layers are known as the troposphere, stratosphere, mesosphere, thermosphere, and exosphere [4]. The divisions between these layers can be determined by their relative elevation from sea level and their average temperatures, which vary due to atmospheric heating [5].

The ionosphere, a part of the atmosphere that is particularly important with regards to this project because it encapsulates the thermosphere; the ionosphere is not one of the five standard layers of the atmosphere mentioned previously [5]. It resides in a region on the very edge of the mesosphere and extends through the last two layers of the atmosphere: the thermosphere and exosphere.

While there is still speculation on the specifics of its range, it is commonly believed that it exists between 70 and 1,000 km above the Earth's surface [6]. The ionosphere derives its name from the high concentration of ions – particles that have either gained or lost electrons – that are contained within its boundaries.

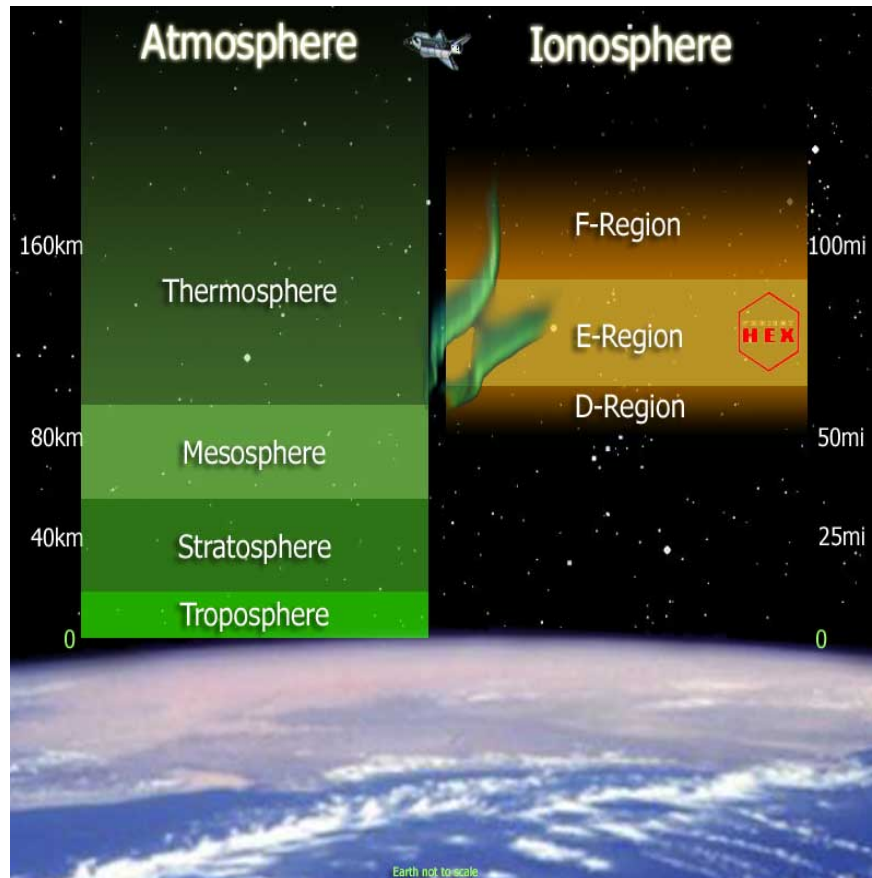


Figure 2.1: Earth's Ionosphere has multiple layers of interest. [7]

It has been observed that the heating events occurring in the ionosphere can influence radio waves, even causing destructive interference on certain frequencies [6]. The ionosphere is composed of three main layers: the D layer, the E layer and the F layer [6].

The D layer exists within 70 to 90 km above the surface of Earth [6]. During Earth's night cycle, the number of free electrons in the D layer is greatly reduced allowing radio waves to propagate through the D layer with relatively little signal strength reduction. However, during Earth's day cycle it has been proven that radio waves are reflected by the D layer due to the emergence of more free electrons in this region [6].

The E layer extends from 90 to 160 km above the surface of Earth [6]. In both the day and night cycles ionization of free electrons exist in this region causing radio waves of low frequencies to be reflected [6].

The F layer extends from 160 km to the end of the ionosphere region [6]. It has a large

concentration of free electrons and is mainly responsible for the heating in our atmosphere, as the majority of the thermosphere is contained within this region. This layer is able to reflect all signals lower than 30 megahertz [6].

The region above the ionosphere, known as the magnetosphere, is the region surrounding a planet where the natural magnetic field of the planet interacts with, and often deflects, solar winds and other charged space particles [8]. The pressure on the Earth's magnetosphere from the flux of charged particles emitted from the Sun (the solar wind), compresses the magnetosphere and gives it a tail-like shape that stretches behind the Earth as seen in Figure 2.2 [9].

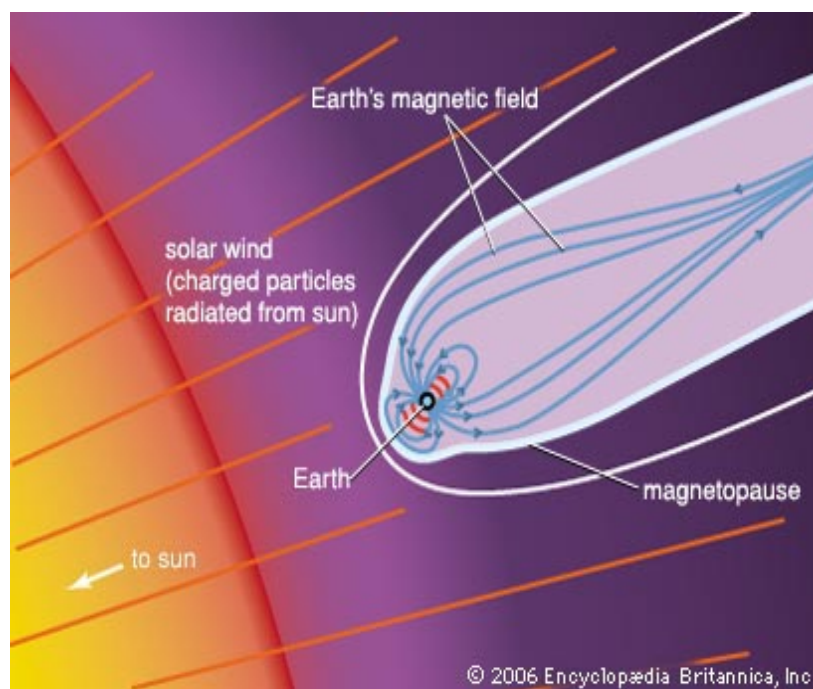


Figure 2.2: Earth's Magnetosphere, Tail Shape Created by Solar Wind [9]

The charged particles that are not deflected and manage to pass through the Earth's magnetosphere collide with oxygen and nitrogen atoms in the upper atmosphere. These collisions knock electrons away from their atoms, leaving ions in an excited state. The resulting ions emit radiation at various wavelengths, creating the colors of the aurora [10]. The region at which this occurs is known as the auroral acceleration region (AAR) [11].

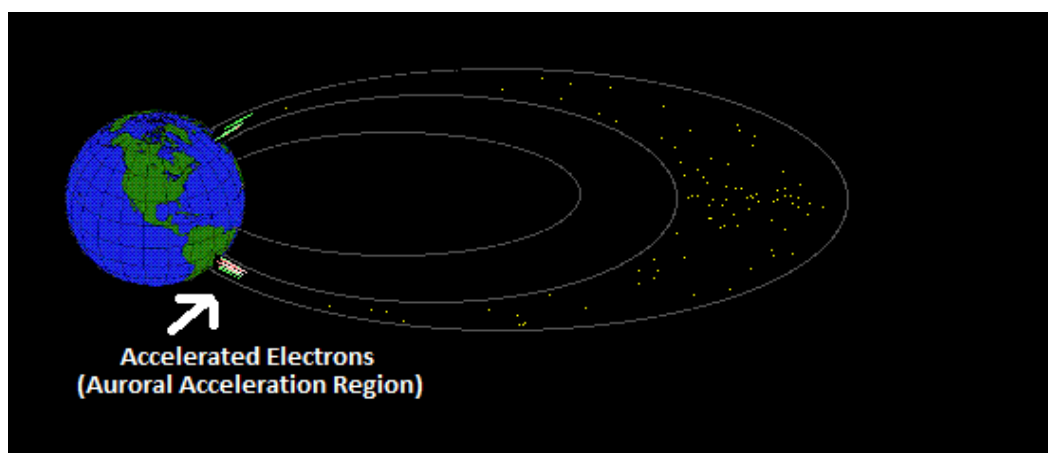


Figure 2.3: Auroral Acceleration Region [11]

2.2 Space Weather and its Effects on Earth

Space weather, which includes solar winds, is the general name for conditions in space that are caused by the Sun [12]. Magnetic storms, a part of space weather, are a series of geospace disturbances. These storms can cause many effects such as the aurora, radio and television interferences, hazards to orbiting astronauts and spacecrafts, and even power grid failures [13].

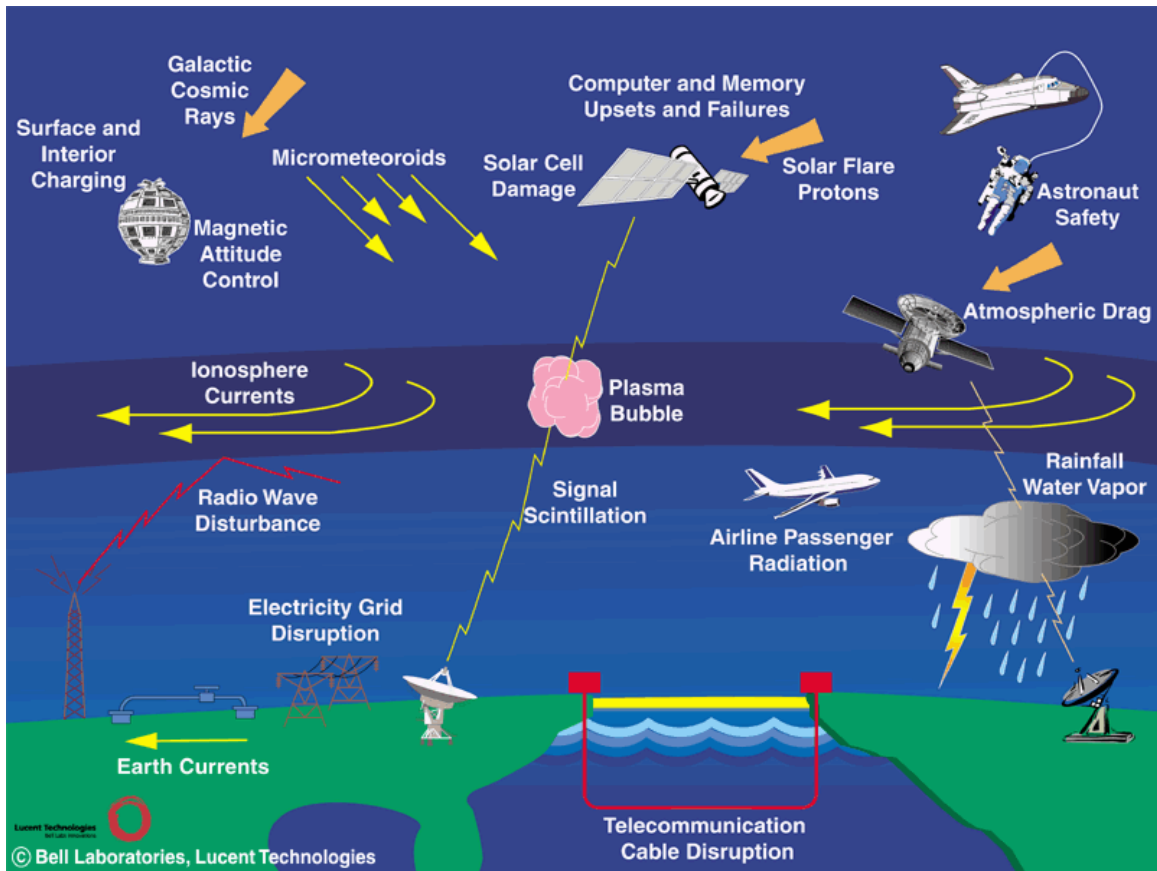


Figure 2.4: Earth's Ionospheric Phenomena [14]

Figure 2.4 displays various effects caused by ionospheric currents in Earth's atmosphere. Due to the increasing number of satellite information systems, high altitude spacecraft travel, and the expansion of electric power grids, society is becoming increasingly susceptible to the effects of space weather.

The National Space Weather Program (NSWP) is an initiative founded to “achieve an active, synergistic, inter-agency system to provide timely, accurate, and reliable space weather warnings, observations, specifications, and forecasts” [13]. To develop a prediction system, the NSWP uses models of the global temperature, circulation, and density of the thermosphere. However, modeling the density and circulation of the thermosphere requires knowledge of the energy inputs from solar winds, which have not yet been quantified. This four-year project proposes to take steps toward solving this problem and quantifying the Sun's energy input to the thermosphere by fitting a model directly to measurements of the energy input as recorded by the FAST satellite.

2.3 Fast Auroral SnapshoT (FAST) Satellite

The Fast Auroral SnapshoT (FAST) Explorer was launched on August 21, 1996 into a 350 km by 4175 km elliptical orbit, inclined 83° [1]. While traveling along its orbit, the FAST satellite continuously spun in a reverse cartwheel direction along its spin axis. It crossed through the auroral zones four times per orbital period, which lasted 133 minutes [15]. The FAST satellite successfully recorded data until its instruments began to fail on January 1, 2000.

Passing through four auroral zones each orbit, the FAST satellite collected various types of data relevant to the study of the micro-physics of space plasma and accelerated particles, which cause the aurora [16]. The FAST satellite, which can be seen in Figure 2.5, was equipped with various instruments including magnetic sensors (flux-gate magnetometer and search coil magnetometer), electric field detectors (Langmuir Probes, generally in pairs), and ion and electron analyzers [17]. Upon launch one of the electric field detectors failed to deploy correctly preventing data from being recorded along the spin-axis of the satellite.

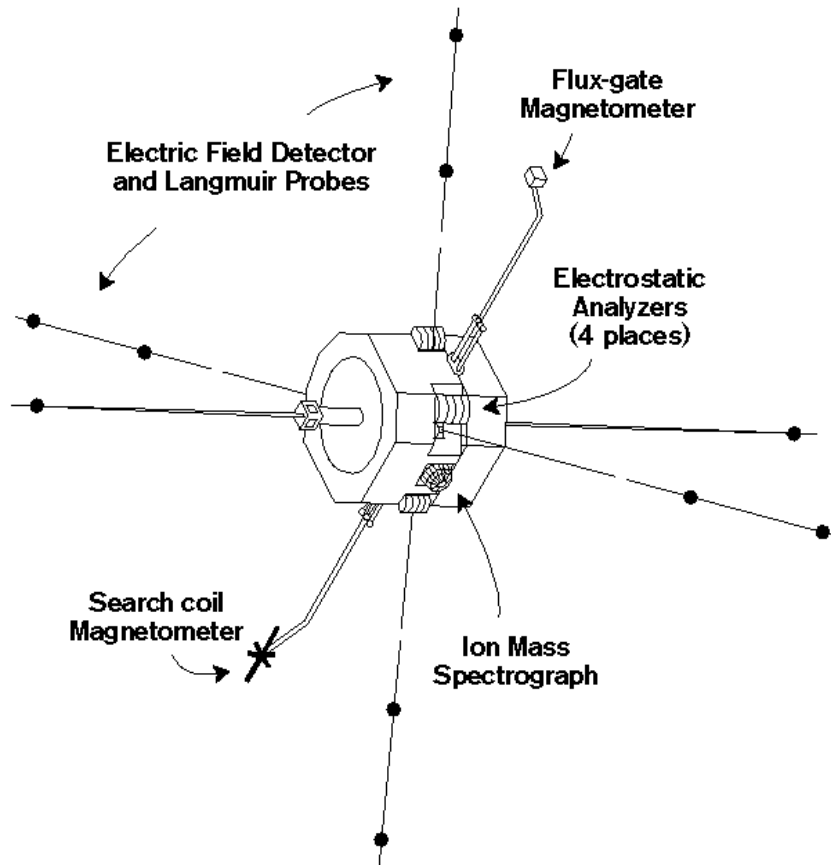


Figure 2.5: FAST Instruments [15]

These instruments, which collected measurements in real-time, allowed the satellite to measure the electric and magnetic fields, plasma waves, energetic electrons and ions, ion mass composition, and thermal plasma densities and temperatures in the auroral regions.

In addition to data collection, the instruments on-board the FAST satellite also served to keep the satellite along its required orbit. Nominally the satellite should spin in a reverse cartwheel direction on its spin axis while traveling in an elliptical orbit around the Earth. To ensure that the satellite remained on its elliptical orbit, the attitude control systems of the FAST satellite would alter the orientation of the satellite to match its desired orbital path.

High resolution data collection on the FAST satellite was triggered by the detection of high fluctuations of either the electric or magnetic field, such as density cavities or ion beams. When an event was detected, the sampling rate of the data collection was switched from a slow survey to high-speed burst memory mode in order to allow for adequate data sampling while avoiding

overflowing the memory with non-consequential samples [16]. Normally burst mode had a higher sampling rate (approximately 16kHz) compared to survey mode which was generally 1-2 orders of magnitudes slower [17].

The FAST satellite was able to measure various fields such as electric potential, magnetic field data, and ion and electron flux. The data measured by the FAST satellite was in the form of raw unprocessed data.

2.4 Accessing FAST Satellite Data

The data collected by the FAST satellite was initially transmitted to the NASA Goddard Space Flight Center where it was then routed to the Science Operation Center (SOC) at the University of California, Berkeley [17]. The SOC is the main center for scientific analysis of the data collected by FAST. It is also responsible for serving as an online database for all FAST data, allowing researchers the ability to access various recorded data such as magnetic and electric field. Using the Satellite Data Tool and Interactive Data Language routines it is possible to access the FAST satellite data remotely from the SOC servers.

Satellite Data Tool

The Satellite Data Tool (SDT) is a program created by UC Berkeley engineers that enables remote access to the servers at the SOC [17]. Developed in the mid-1990s, SDT was created to enable fast access of data collected by various satellites in real-time. This software was originally designed to work under UNIX or Linux, but was later ported over to Solaris systems – which was used at SRI. The SDT enables access to data obtained from the FAST, Polar, Cluster, Geotail, THEMIS, ISEE, and CRRES missions [17].

SDT Software Diagram

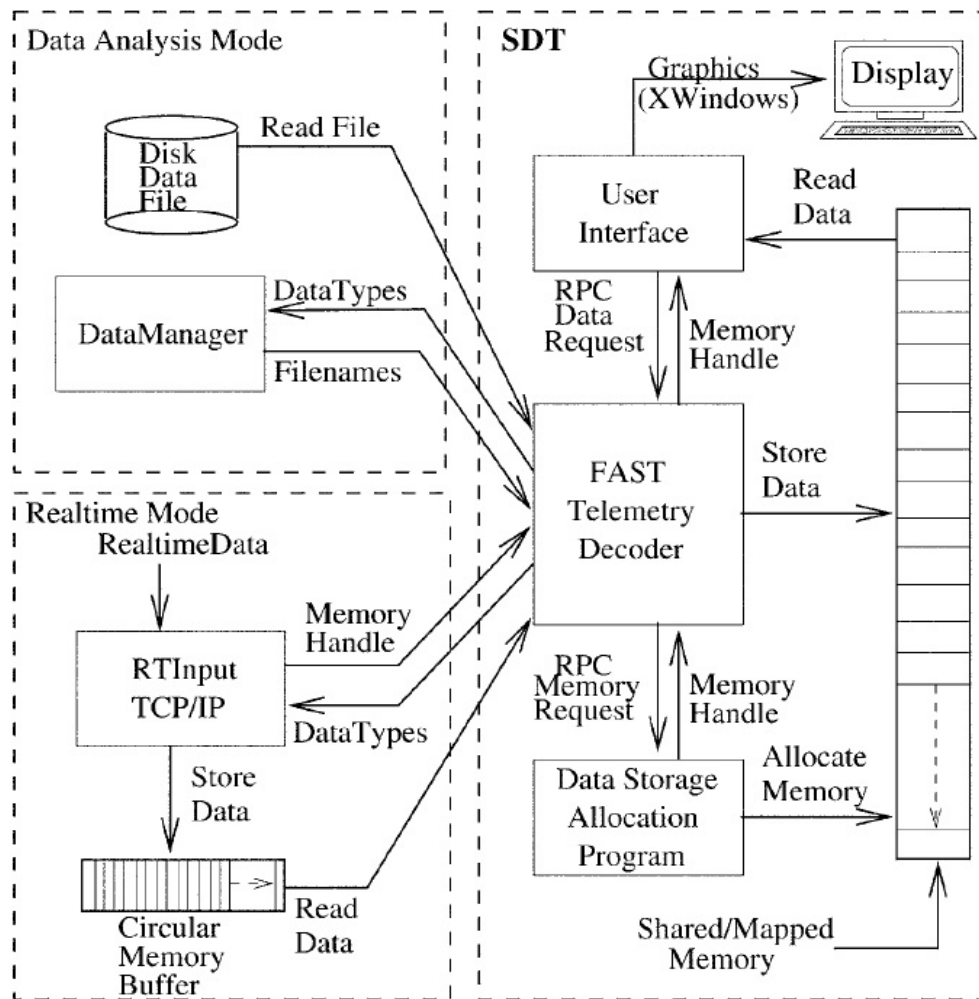


Figure 2.6: SDT Software Design Diagram [17]

The SDT is used as a medium to obtain the raw data collected by the FAST satellite during the course of its many thousands of orbits. Once data from a desired orbit is downloaded from the SOC, SDT's telemetry decoder decommutates the data and stores it into a shared memory buffer that can then be accessed by Interactive Data Language routines [17]. At the time of this writing only a single user can have access to the same install of the SDT on a machine at a time.

Interactive Data Language

Interactive Data Language (IDL) is a programming language used primarily for data analysis. IDL is dynamically typed and specialized for vector operations, which makes it very efficient for processing large amounts of data. It takes constructs from both FORTRAN and C, but more closely resembles the syntax of FORTRAN.

IDL was originally intended to be used in conjunction with SDT to offer scientists the flexibility of being able to build their own data analysis tools without having to directly manipulate the SDT software. Once the data is downloaded from the SOC remote servers and stored in the SDT shared memory buffer, IDL can access its contents by using a function call that points to the specific fields data. This fields data is referred to as a Data Quantity Definition (DQD).

There are two stipulations for the correct data to appear in IDL from SDT: the plots of the desired data must first be displayed in SDT and the time-span of the data must be specified correctly so that reasonable data is outputted. Once the data is extracted, it is either preprocessed in SDT using IDL routines or directly exported to a Common Data Format file.

Common Data Format

Once exported from the SDT using IDL routines, the preprocessed FAST data is saved to Common Data Format (CDF) files. CDF files have built-in support for data compression and can support large file sizes. This format was introduced by NASA to allow for the easy storage and access of multidimensional data. The structure of a CDF file is essentially a multidimensional matrix that stores each data component within a column of the matrix, with each element of the matrix having the capability to store multiple data values as seen in Figure 2.7.

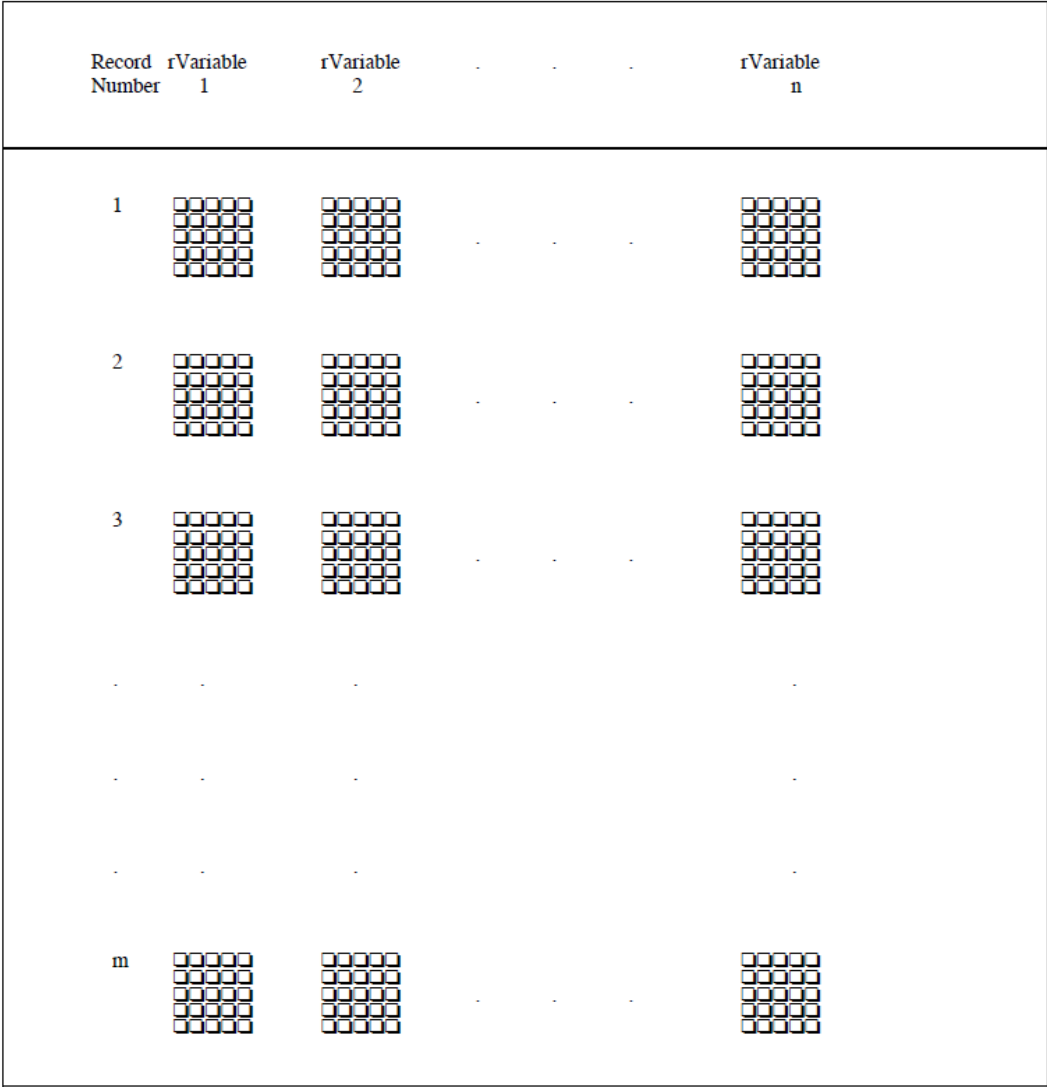


Figure 2.7: Conceptual View of CDF Files [18]

Each row of data stored in a CDF file needs to be time stamped with an Epoch or UNIX Time for the data to be considered valid. The primary motivation behind exporting the data in CDF files is to allow for ease of interfacing with MATLAB, which has efficient built in functionality to read in CDF files.[19].

2.5 Coordinate Systems Represented by the FAST Data

The FAST satellite data that is exported using the SDT and IDL routines is separated into six main CDF files corresponding to the six main data types collected by FAST: positional, magnetic field, electric field, spin axis, electron energy flux, and ion energy flux. Although these six files contain all of the data necessary to calculate the Poynting and kinetic energy flux, the data types within each file are represented with respect to one of the following three different coordinate systems: Geocentric Equatorial Inertial Coordinate System, Equatorial Coordinate System, or Data Coordinate System 2. In order to work with the data, the data in each file must first be converted into a single unified coordinate system. To interpret the Poynting and kinetic energy flux calculations with respect to the Earth, the Geocentric Coordinate System (GEO) was chosen as the unifying system. In total, four unique coordinate systems were handled throughout the entirety of this project. For additional information on these as well as other relevant coordinate systems and their transformations, please refer to the 2010 SRI MQP report [20].

Geocentric Equatorial Inertial Coordinate System (GEI)

The geocentric equatorial inertial (GEI) coordinate system is a Cartesian coordinate system designed to map out areas around and outside the Earth's atmosphere with respect to the Earth's position in space. In the GEI coordinate system the rotation of the planet has no influence on the coordinates of objects in free space; however, the rotation does influence the coordinates of objects resting on the surface of the Earth. Figure 2.8 shows the orientations of the X Y and Z-axes.

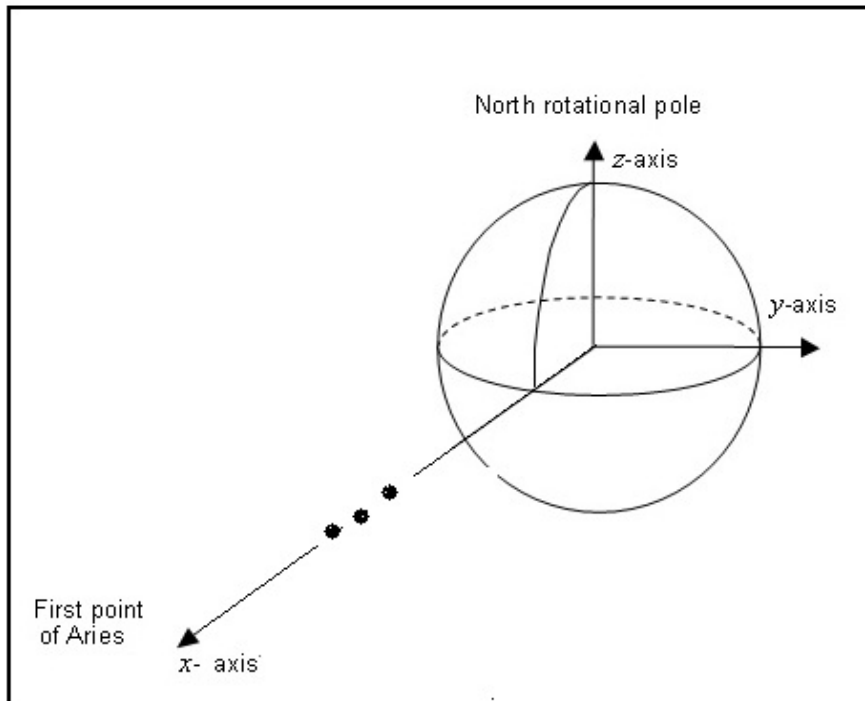


Figure 2.8: Geocentric Equatorial Inertial Coordinate System (GEI) [20]

The origin of the GEI system is located at the center of the Earth. The Z-axis is positive through the Earth's geographic North Pole and the X-axis points positively toward the first star in the Aries constellation through the Earth's equator. The Y-axis is the cross product of the X and Z-axes and projects out of the equator [20].

Equatorial Coordinate System (ECS)

The Equatorial Coordinate System (ECS) is the spherical version of the GEI coordinate and consists of two angles, which map the spin axis of the satellite: the right ascension angle and the declination angle. The right ascension angle begins at the Vernal equinox, also known as the location of Earth's orientation that points to the first star of Aries, and increases eastward. The declination angle begins at the equator and points to the North celestial pole [17]. Figure 2.9 shows a visual representation of these spin axis components.

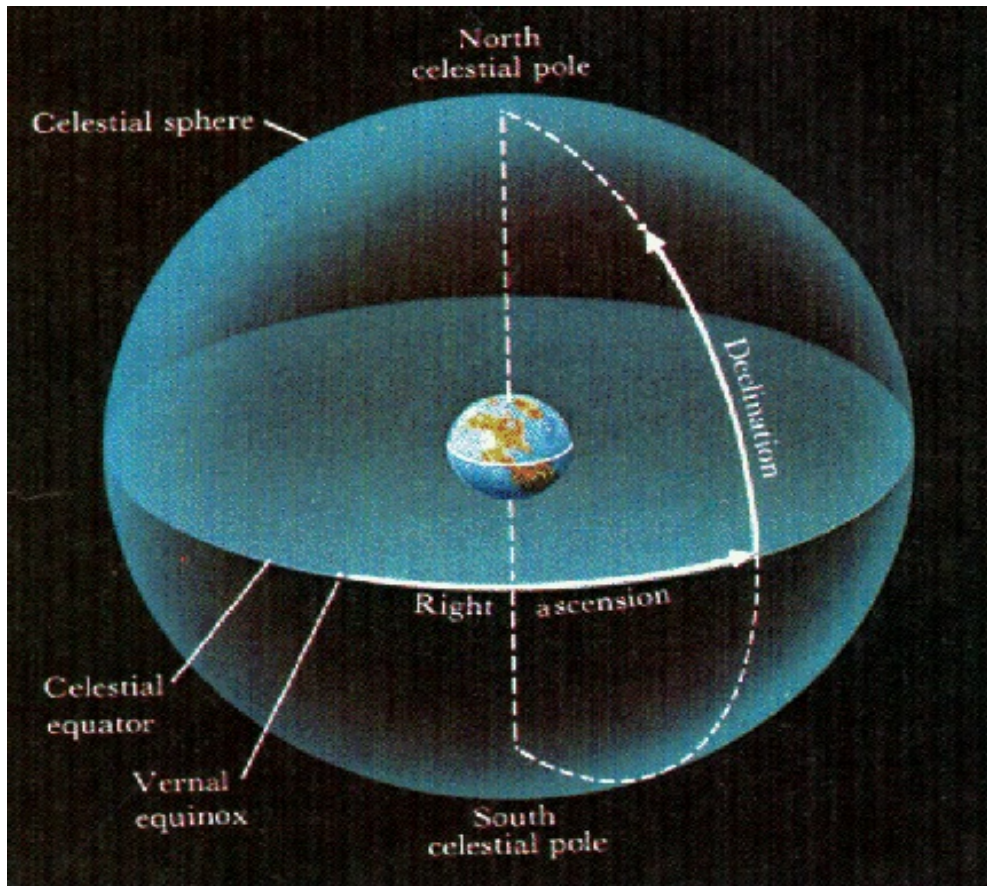


Figure 2.9: Equatorial Coordinate System (ECS) [21]

To convert from ECS to GEI (and eventually to GEO), a simple Cartesian to spherical transformation can be completed.

Data Coordinate System 2 (DCS2)

The Data Coordinate System is a Cartesian coordinate system centered at the FAST satellite. The Y-axis of the system goes through the spin-axis of the satellite and is positive to the right of its velocity vector from a perspective of where the satellite once was and the Earth is “down”. The Z-axis is the spin plane projection of the magnetic field onto the spin plane of the satellite. The X-axis of the system is the cross product of the Y and Z-axes and is generally along the velocity vector of the spacecraft.

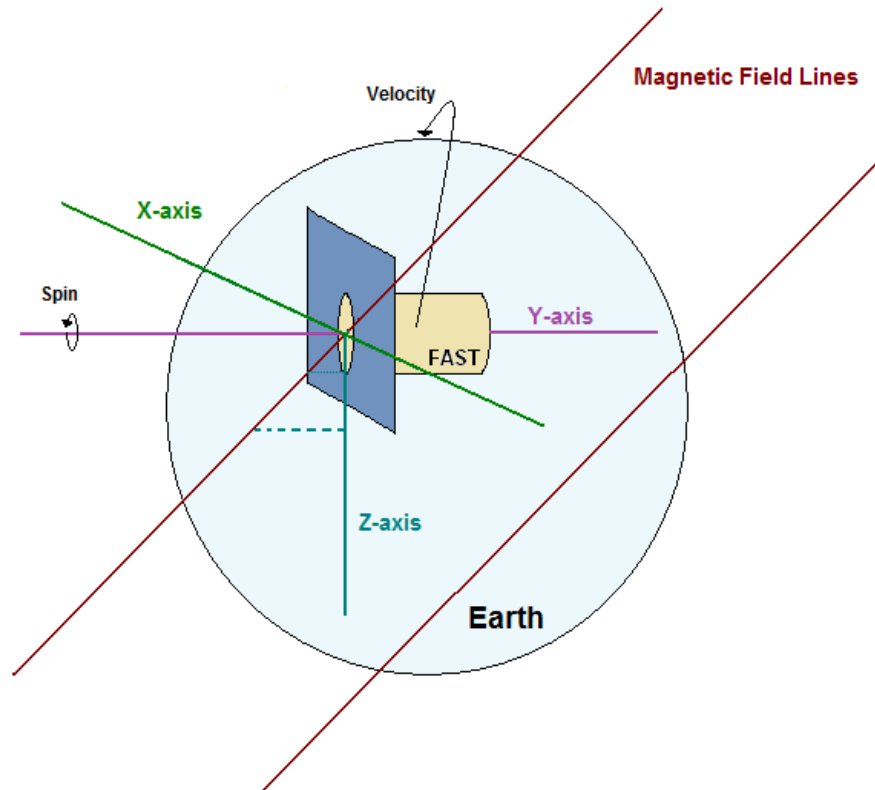


Figure 2.10: Data Coordinate System 2 (DCS2)

DCS2 is an alternative version to the original Data Coordinate System (DCS) used by the 2010 MQP. The main difference between the two versions is that the Y-axis in DCS was positive with relation to the westward direction of the Earth. This caused the X and Y-axes to flip polarities whenever the satellite crossed the north and south poles, which does not occur in DCS2 [20].

Geocentric Coordinate System (GEO)

The geographic geocentric (GEO) coordinate system is very similar to the GEI coordinate system. Both GEI and GEO are Cartesian coordinate systems with origins located at the center of the Earth and their Z-axes positive through the geographic North Pole. The primary difference between the two systems is that the X-axis for each system points to a different location. The GEO coordinate system rotates along with the surface of the Earth whereas the GEI coordinate system remains stationary as the Earth rotates. The Greenwich Hour Angle, or the angle between the X-axis of

both systems, can be used to convert between the GEI and GEO coordinate systems [20].

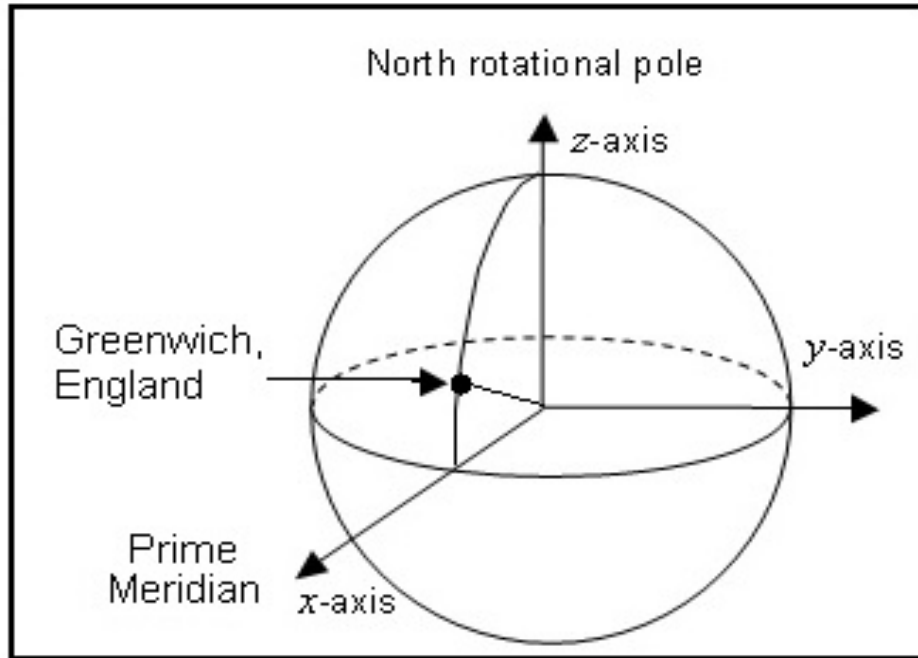


Figure 2.11: The Geocentric Coordinate System (GEO) [22]

The X-axis in the GEO coordinate system is positive through the intersection of the equatorial plane and the prime meridian (0° longitude). The Y-axis of the coordinate system is obtained by taking the cross product of the Z and X-axis. [20]

2.6 Poynting and Kinetic Energy Flux

Processes that occur in Earth's auroral region are primarily due to the effects of Joule heating. Joule heating, which can be described as the product of the electric field and the height-integrated current density ($E \cdot J$ ($\frac{W}{m^2}$)), is a high-altitude phenomenon that occurs when the drift energy of the ionospheric ions turns into thermal and kinetic energy due to particle collisions [23]. Joule heating in Earth's ionospheric region can be quantified by estimating the field-aligned Poynting flux; however, there is evidence to suggest that in the auroral acceleration region (AAR), the Poynting flux is redistributed across field lines and is partially converted to kinetic energy flux. This relationship can be seen in Figure 2.12, which shows data measured by a rocket passing

through Earth's ionosphere.

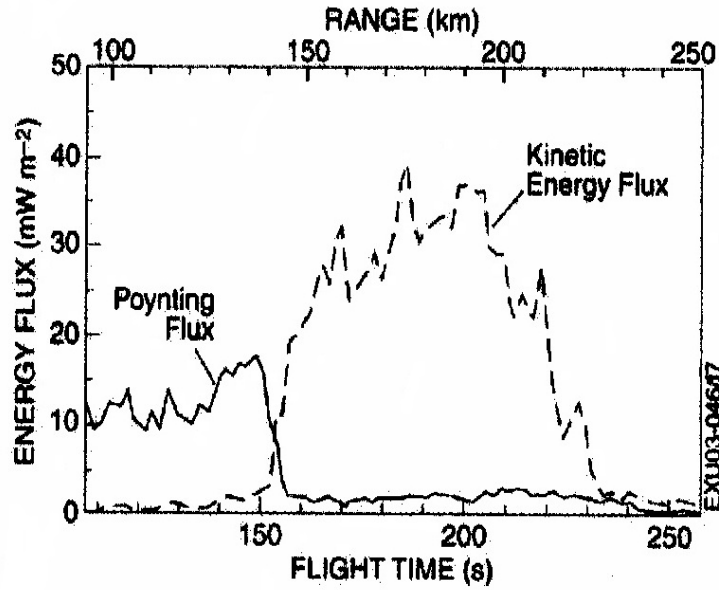


Figure 2.12: Complementarity nature of Poynting and kinetic energy flux as observed by a rocket flying under the boundary of the auroral arc [1]

Thus, in order to obtain the Joule heating factor in the AAR, the Poynting and kinetic energy flux need to be calculated. The four-year proposal of this project aims to model the relative spatial distribution of Poynting and kinetic energy flux below the AAR [1].

Poynting Flux The Poynting vector is used as a common measurement of the rates of flow of energy and momentum in electromagnetic waves (e.g. in analysis of electromagnetic radiation) and is used to calculate the energy flux ($\frac{W}{m^2}$) of an electromagnetic field. The general formula is defined as [1]:

$$S_{||} = \frac{(\mathbf{E}_{\perp} \times \delta \mathbf{B})}{\mu_0} \quad (2.1)$$

For ionospheric measurements \mathbf{B} represents the sum of the main geomagnetic field. The perturbation of the geomagnetic field, $\delta \mathbf{B}$ (Tesla), is the difference between the measured geomagnetic field and a modeled geomagnetic field known as the International Geomagnetic Reference Field (IGRF). These fields lines are predominantly horizontal [24]. Due to its orthogonality to the main

geomagnetic field, the electric field, \mathbf{E}_\perp ($\frac{\text{volts}}{\text{meter}}$), is primarily perpendicular to \mathbf{B} [24]. The value μ_0 is the permeability of free space. Finally, the resulting value \mathbf{S}_\parallel is the calculated Poynting flux, which is in a direction parallel to the geomagnetic field that the satellite is traveling along known as \mathbf{B}_0 [1].

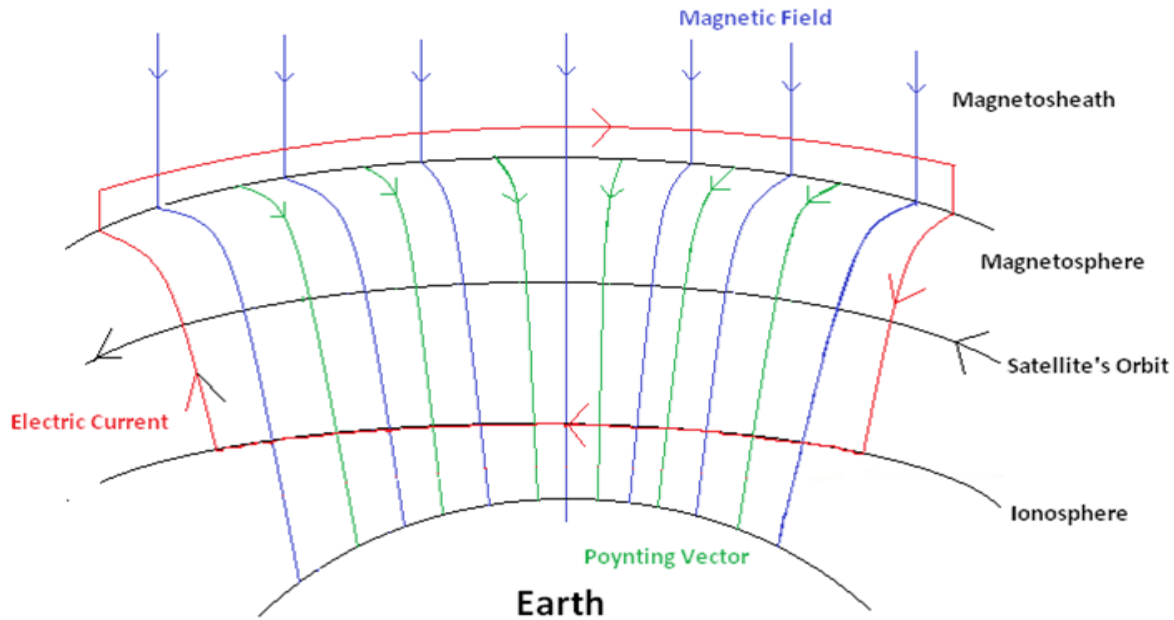


Figure 2.13: The Poynting vector and Magnetic Field Lines, Respective to Altitude

The Poynting flux represents the flow of energy through an area. The direction that the vector points to corresponds to the direction of the energy flow and the magnitude corresponds to the intensity (flux). Thus the Poynting flux ($\frac{W}{m^2}$) can be described as the total amount of energy held by an electromagnetic wave traveling through a surface [25]. This is useful for quantifying the amount of heat that is dissipated in Earth's ionosphere due to Joule and particle heating [1].

Kinetic Energy Flux The total kinetic energy flux of electrons and ions can be calculated by taking the summation of the kinetic energy for all up-going (from the magnetosphere to the ionosphere) and down-going (from the ionosphere to the magnetosphere) electrons and ions [20]. The kinetic energy flux is used to describe the rate of energy transfer by ions or particles through an area and is also measured in ($\frac{W}{m^2}$).

2.7 Geophysical Parameters

This year's project worked to develop functions, which produce binned statistical models of the average Poynting and kinetic energy flux. These models can be limited based on the following geophysical parameters [1]: altitude, magnetic local time, invariant latitude, and the Kp and ap index. These limiting parameters can be set by the user of the function to allow for analysis of specific occurrences of Poynting and kinetic energy flux in Earth's atmosphere.

Altitude

The Poynting flux calculations were completed using the assumption that the electric field is generally perpendicular to the magnetic field; however, at high altitudes this assumption does not hold true. Therefore, altitude is used as a limiting parameter for the binned statistical models to account for the higher chance of error in the Poynting flux calculations present at higher altitudes.

Magnetic Local Time

Magnetic local time (MLT), which is longitude with respect to Earth's magnetic poles (magnetic longitude) measured in hours instead of degrees, provides a perspective of the Earth that is relative to the position of the Sun. For example, the point of magnetic longitude that is directly facing the Sun at any given time is always considered 12:00 pm MLT. This is an appropriate limiting parameter for the binned statistical models because the intensity of the Poynting flux is dependent on the position of the Sun. During MLT daytime hours, when the intensity of the Poynting flux is generally the highest, the Sun shines directly on the electron and ion particles in the F layer of Earth's ionosphere and causes an increase in Joule heating.

Invariant Latitude

Invariant latitude (ILAT) is latitude with respect to Earth's magnetic poles, or magnetic latitude, mapped to the surface of the Earth. ILAT is used as a parameter in the binned statistical models to provide insight into the locations around the Earth at which the highest instances of Poynting and kinetic energy flux occur. For example, a higher intensity of Poynting and kinetic energy flux should be visible in the AAR, which is located in areas of high north and south magnetic latitudes.

***aP* and *Kp* Indexes**

The *Kp* index is a measure of geomagnetic disturbances calculated by taking the mean of the values recorded at thirteen substations near the auroral region. The *Kp* index is measured in three-hour intervals and increases as a function of the observed geomagnetic disturbance. As seen in Figure 2.14, the *Kp* index is not represented in integer values.

<i>Kp</i>	0 _o	0+	1-	1 _o	1+	2-	2 _o	2+	3-	3 _o	3+	4-	4 _o	4+
<i>ap</i>	0	2	3	4	5	6	7	9	12	15	18	22	27	32
<i>Kp</i>	5-	5 _o	5+	6-	6 _o	6+	7-	7 _o	7+	8-	8 _o	8+	9-	9 _o
<i>ap</i>	39	48	56	67	80	94	111	132	154	179	207	236	300	400

Figure 2.14: *Kp* index with matching *ap* index [2]

The *ap* index directly corresponds to the *Kp* index; however, unlike the *Kp* index it is the defined as a integer value. As with the *Kp* index the *ap* index measures the amount of geomagnetic disturbance in the auroral region. The *ap* index is used as a parameter for the final polar plot visualization to allow for the specific viewing of the Poynting flux during periods of high or low geophysical disturbances in Earth's atmosphere.

Chapter 3

Methodology and Implementation

Below (Figure 3.1) is a block diagram that illustrates the inputs and outputs of the system implemented. Each of these blocks will be fully detailed in later sections.

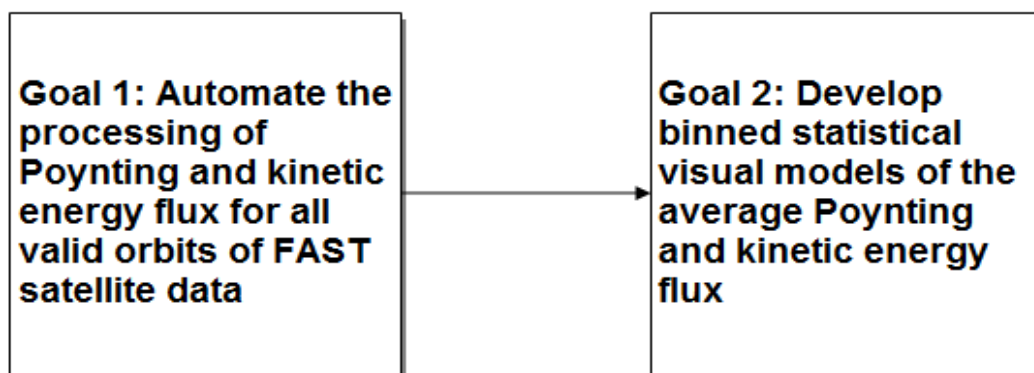


Figure 3.1: Top Level Block Diagram

The automation of Poynting and kinetic energy flux processing (Goal 1) required downloading preprocessed data compiled by the University of California, Berkeley and performing further calculations in MATLAB to obtain the Poynting and kinetic energy flux for each orbit.

Due to an error in the preprocessed electric and magnetic field components contained within the UC Berkeley data, several steps were taken to re-calculate and re-preprocess the electric and magnetic field components. This required downloading the raw satellite data from remote servers hosted by UC Berkeley using the Satellite Data Tool (SDT) and completing the required preprocessing with a new set of Interactive Data Language (IDL) routines.

An additional complication in processing the Poynting and kinetic energy flux arose with accounting for a missing electric field component that was not recorded as a result of sensor on the

FAST satellite that failed to deploy. Recovery of the missing component was attempted as it would offer a more accurate measurement of the average Poynting and kinetic energy flux.

The final statistical models (Goal 2) were created through a process of binning and averaging the Poynting and kinetic energy fluxes calculated in completion of the first goal of this project. The models were limited by series of geophysical parameters to allow for analysis of specific occurrences of the Poynting and kinetic energy flux within Earth's atmosphere.

3.1 Automate the Processing of Poynting and Kinetic Energy Flux

In completion of the first goal of this project, five main steps were accomplished. The block diagram in Figure 3.2 shows the progression of these steps.

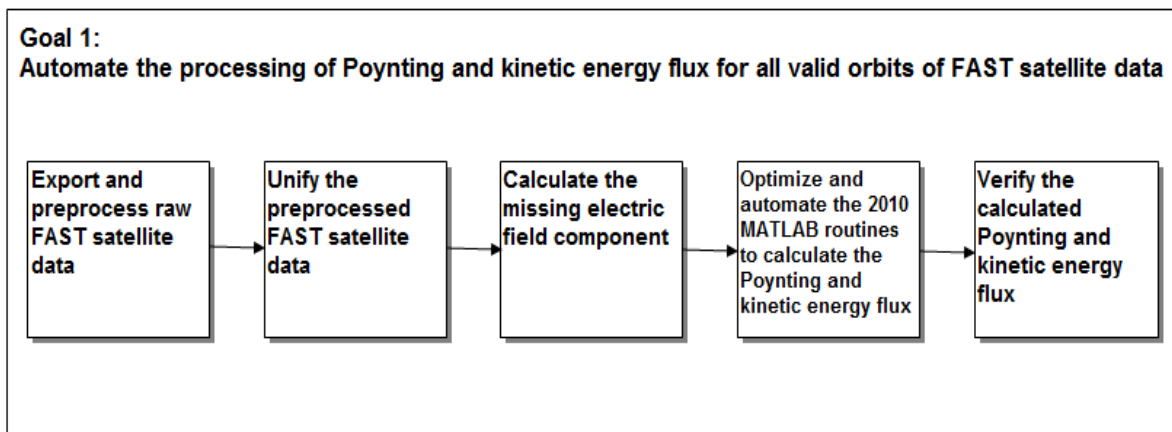


Figure 3.2: Goal 1 Top Level Block Diagram

Researchers at the University of California, Berkeley preprocessed raw data measured by the FAST satellite and made it available for general use by the public. However, in 2010 communication with Dr. Robert Strangeway of the University of California, Los Angeles revealed that while the preprocessed positional data was correct, the electric and magnetic field data was unreliable due to errors in calculation. Therefore, to accomplish the first goal of this project and correctly calculate the average Poynting and kinetic energy flux, the raw FAST satellite data had to be accessed and re-preprocessed. Using the Satellite Data Tool (SDT), a software suite that enables

fast, real-time access to data collected by various satellites, the raw FAST data was successfully downloaded from remote servers maintained by UC Berkeley. Using updated Interactive Data Language (IDL) routines originally developed by researchers at UC Berkeley and UCLA, the FAST data was re-preprocessed and exported into Common Data Format (CDF) files. Using the original preprocessed positional data as a basis for comparison, the exported data was verified to be correct; however, further verification on the accuracy of the re-preprocessed magnetic and electric field data is currently pending.

Working under the assumption that the magnetic and electric field data were re-preprocessed correctly, 20,000 satellite orbits worth of data were preprocessed and exported using the SDT and IDL routines. Data exported from SDT was separated into six CDF files per orbit: positional, magnetic field, electric field, spin-axis, electron, and ion data. These six data types exported from SDT were represented in various coordinate systems, resolutions, and were recorded over varying time periods. Additionally, the electric and magnetic field data contained many outliers, which could potentially skew and calculated results. Therefore, outlier removal and unification of the coordinate systems, resolutions, and time ranges of all data in each orbit was completed in MATLAB to allow for the accurate representation of the final Poynting and kinetic energy flux calculations.

Due to a malfunctioning sensor, the FAST satellite was unable to record electric field data along its spin axis. In addition, the electric field data recorded along the magnetic field was deemed unusable due to an excess amount of noise within the signal. By creating and analyzing binned models of the noisy electric field data plotted against the calculated angle between the magnetic field and the projection of the magnetic field onto the satellite's spin plane, a noise floor level was deduced. Theoretically, by limiting the electric field data recorded along the magnetic field to only those values which fell above the noise floor level, recovery of the unrecorded component was feasible through use of trigonometric functions. However, by creating several binned models of the electric field data it was observed that for different ranges of orbits the noise floor level appeared to change. Lacking an efficient method to determine the correct noise floor level for each orbit, the Poynting and kinetic energy flux was calculated with the electric field components along the magnetic field and the satellite's spin axis set to zero.

Continuing on the progress made by the 2010 MQP, MATLAB routines were developed that

are able to automatically calculate the Poynting and kinetic energy flux for a given range of FAST satellite data. These routines, which were optimized to efficiently work with nearly 20,000 orbits worth of valid FAST data, automatically preprocess and unify the FAST data before completing the Poynting and kinetic energy flux calculations. Using these routines, a database of Poynting and kinetic energy flux for all valid orbits of FAST data can be created.

Finally, to verify that the Poynting and kinetic energy flux had been correctly calculated, the results were compared against data collected by the Sondrestrom radar located in Kangerlussuaq, Greenland. Due to the limited time frame of this project, only a select number of orbits were compared against the radar data. The results from these limited comparisons indicated that the calculated Poynting flux data looks promising; however, final verification is currently pending.

The methods used to complete the five main steps of Goal 1 are described in further detail in the following sections.

3.1.1 Export and Preprocess Raw FAST Satellite Data

The first step in completing Goal 1 of this project was to correctly export and preprocess raw FAST satellite data from the Satellite Data Tool (SDT) using Interactive Data Language (IDL) routines.

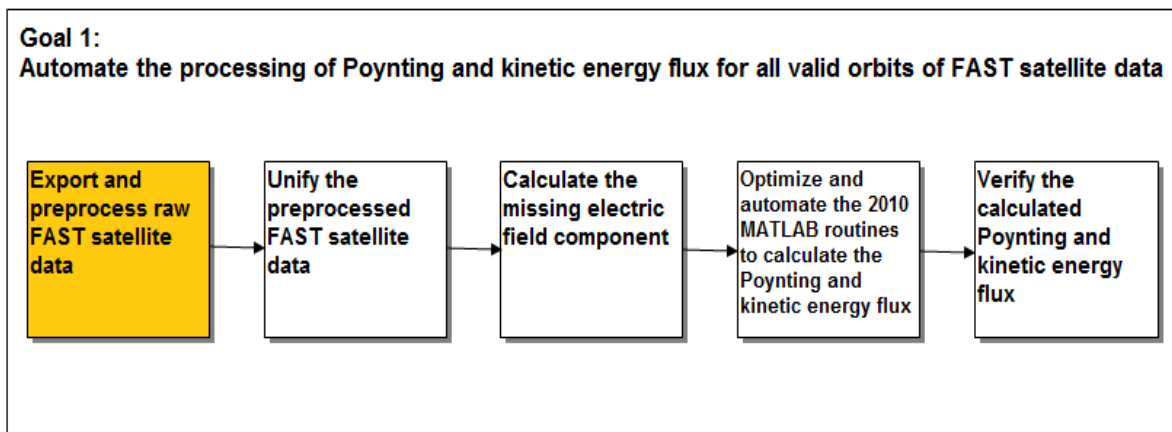


Figure 3.3: Goal 1 Block Diagram, Step 1

At the time of this publication the Satellite Data Tool can only be installed on a Solaris or UNIX/Linux server machine. In order to access SDT on a non-Solaris or UNIX/Linux server machine, a Secure Shell (ssh) can be used. This project was completed on Windows machines,

which required the use of a program called Xming to launch a Secure Shell connection. Once connected to a machine, SDT and IDL can be launched from the command-line interface. SDT must be launched prior to launching IDL so that data can be loaded into the shared memory buffer.

The raw FAST data was downloaded from SDT in two ways: individual and batch. When downloading FAST satellite data on an individual orbit basis, the Data Manager Tool program was used to send data retrieval requests to the SOC remote servers, and subsequently download the data directly to the user's local disk. When using the Data Manager Tool, the machine sending the data retrieval request must be certified by the SOC remote servers in order to download the data. When downloading FAST satellite data on a batch scale the Network Data Facility was used to download the files for a specific orbit range without requiring certification. Figure 3.4 shows an example of the interface of the Network Data Facility.

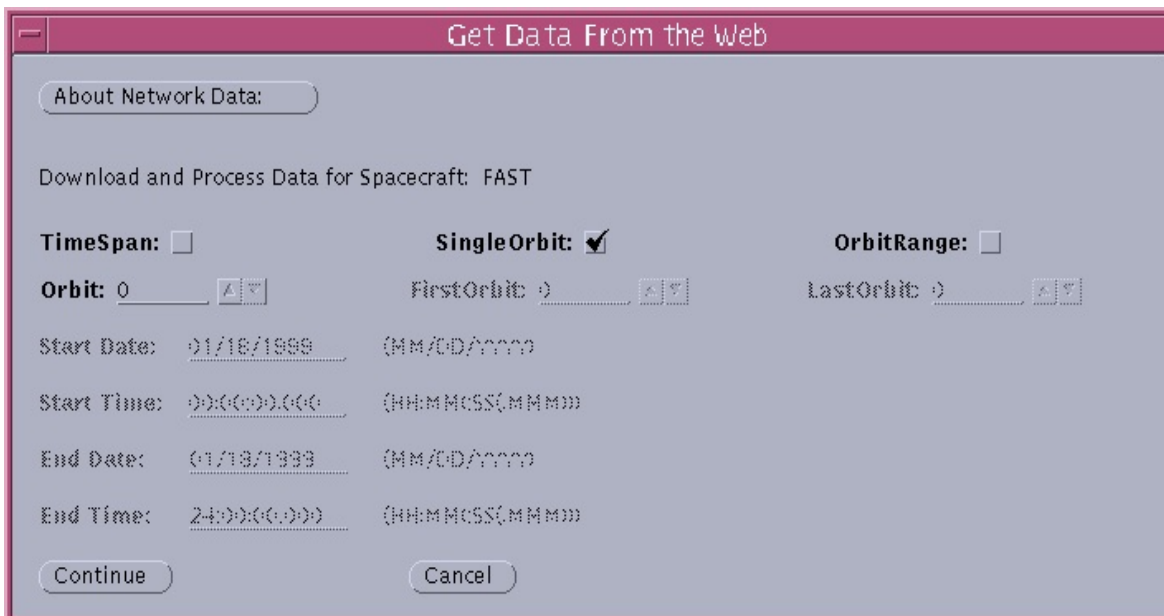


Figure 3.4: Network Data Facility [17]

To preprocess and export the downloaded FAST data, graphs of the raw δB , electric field, orbital, and spin-axis data for the desired orbit had to be displayed in the SDT user interface. Once all of the required data was present, IDL routines were run to preprocess the raw FAST data. Preprocessing consisted of de-spinning the magnetic and electric field data and adjusting it for output. Figure 3.5 shows the raw un-spun magnetic field data displayed in the SDT user interface.

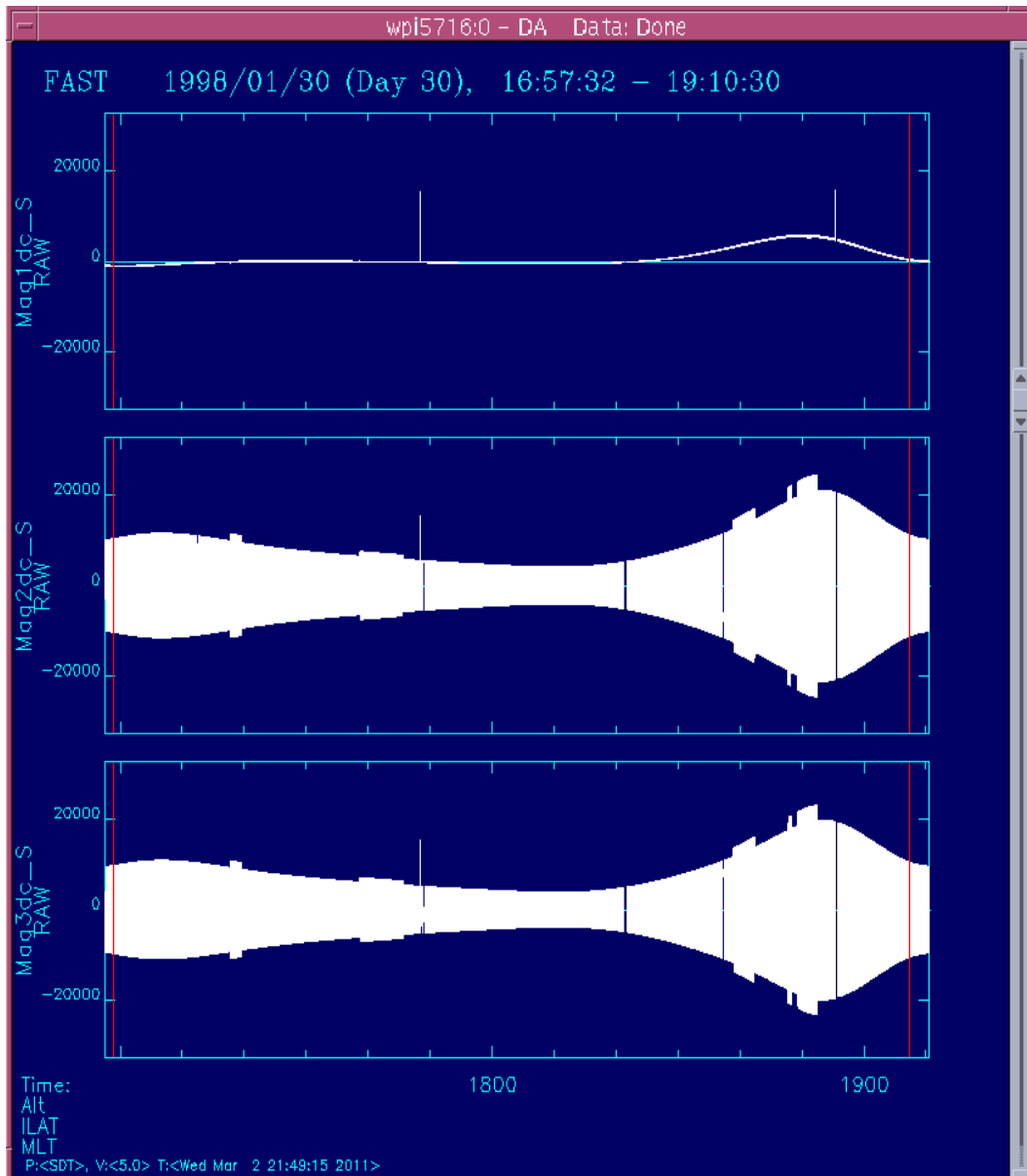


Figure 3.5: SDT Raw Magnetic Field Data

The main IDL routine used to accomplish the preprocessing was `batch_processing.pro`, which called upon several other IDL routines (`ucla_mag_despin.pro`, `fa_fields_despin.pro`, `get_fa_orbit.pro`, `get_fa_attitude.pro`) already included in the SDT IDL library. The `batch_processing.pro` routine preprocessed the electric and magnetic field data and exported it, along with the raw orbital and spin axis data, into Common Data Format files saved into an output directory.

It took approximately five minutes to preprocess and export a single FAST orbit from SDT.

Accordingly, it would have taken nearly twenty-eight full days to effectively process the twenty-thousand orbits needed for this research project given that a single server operated at maximum efficiency and without stall. This was not practical for the scope of this project given its limited time duration and was deemed the bottleneck. To maximize the speed in which the orbits were preprocessed and exported through SDT and IDL, multiple servers were used to effectively speed up the procedure. Separate and unique installations of SDT were installed on each of the three available servers to account for the fact that only one copy of SDT can be running on a single server at a given time by any user.

The electron and ion data used for the calculation of the kinetic energy flux were obtained through different means. Contact with Dr. James McFadden of UC Berkeley revealed that the previously preprocessed electron and ion data were correctly calculated and thus could simply be downloaded through IDL routines, without using SDT.

By running SDT and IDL on all three servers and re-downloading the electron and ion data through solely using IDL, approximately 20,000 orbits of FAST satellite data were successfully preprocessed and exported. This data was saved in a directory called “FAST Data” on a hard drive that was presented to Dr. Russell Cosgrove and Dr. Hasan Bahcivan at the completion of this project.

3.1.2 Unify the Preprocessed FAST Satellite Data

The next step in completing Goal 1 of this project was to unify the preprocessed FAST satellite data exported from SDT by removing outliers and unifying their coordinate systems, resolutions, and time ranges.

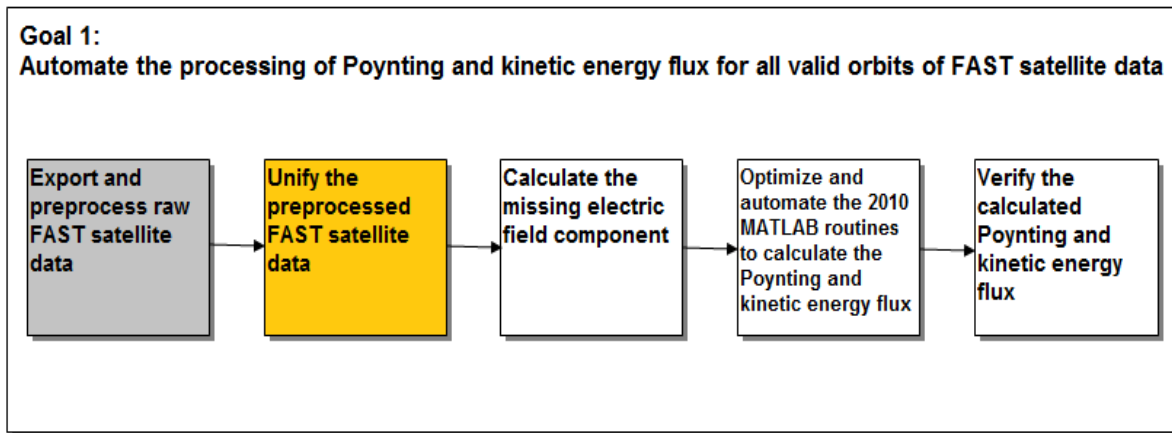


Figure 3.6: Goal 1 Block Diagram, Step 2

Six main data types were preprocessed and exported from SDT to be used in the calculations of the Poynting and kinetic energy flux: positional data, magnetic field data, electric field data, spin axis data, electron data, and ion data. Due to the way the instruments on-board the FAST satellite recorded the data and the way the IDL routines preprocessed the data, all six data types were recorded in various resolutions, time ranges, and coordinate systems. Additionally, the electric and magnetic field data contained many outliers, which could potentially skew the calculated Poynting and kinetic energy flux results. Therefore, before calculating the Poynting and kinetic energy flux, the following processes and transformations were performed on the preprocessed FAST satellite data to ensure that all data types were uniform:

1. Outlier Removal
2. Coordinate System Transformations
3. Correlation of Data Time Ranges and Resolutions

The following sections describe these methods, which were used to unify the preprocessed FAST satellite data.

Outlier Removal

Outlier removal was attempted on a single signal and full orbit basis. For single signal outlier removal, individual outlier data points were removed from an otherwise valid orbit of FAST data;

however, full orbit outlier removal worked to remove outlier orbits whose total data was deemed corrupted and invalid.

Single Signal Outlier Removal The preprocessed electric and magnetic field data exported from SDT was generally very noisy and retained some noticeable outliers as seen in the top plot of Figure 3.7. The cause of these outliers was determined to be primarily due instrumental glitches. In order to remove these outliers an algorithm outlined in “Radar detection of a localized 1.4 Hz pulsation in auroral plasma, simultaneous with pulsating optical emissions, during a substorm”, by Dr. Russell Cosgrove, et. al. was used (refer to Appendix A.1).

Figure 3.7 shows an example of the effectiveness of the outlier removal function when used on a sample of magnetic field data. The top plot shows the original magnetic field signal, while the bottom plot shows the magnetic field signal with outliers removed.

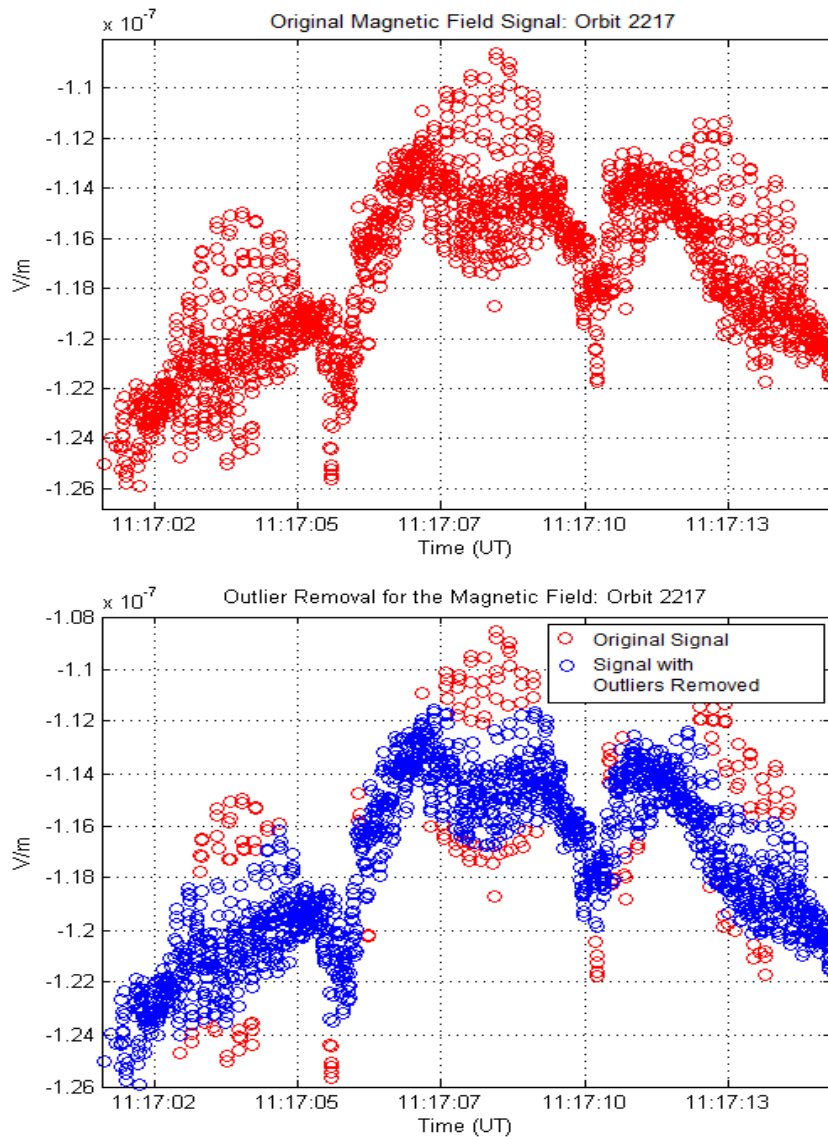


Figure 3.7: Example of Outlier Removal

Orbit Outlier Removal To account for orbits that contained corrupted or invalid data that would not be accurately removed by single signal outlier removal, a function that created histograms was developed to screen for these occurrences. This function allowed for better determination of what data within a range of orbits should be considered outliers; it also aided in the final analysis of trends within the entire orbit range data set. The histogram function is able to take in a series of limiting parameters including a time range, latitude range, longitude range, and altitude range. Based on these input parameters, histogram plots are created representing all data which met the

desired requirements. Through analysis of these histograms a realistic range of acceptable data averages can be determined and outlier orbits with averages that do not fall within this range can be identified.

Figure 3.8 shows a histogram created for the Y-axis δB data of all latitude, longitude and altitude ranges over a three day period. As seen below, the data is centered around 0 nT; however, outliers are present towards the outer edges of the plot.

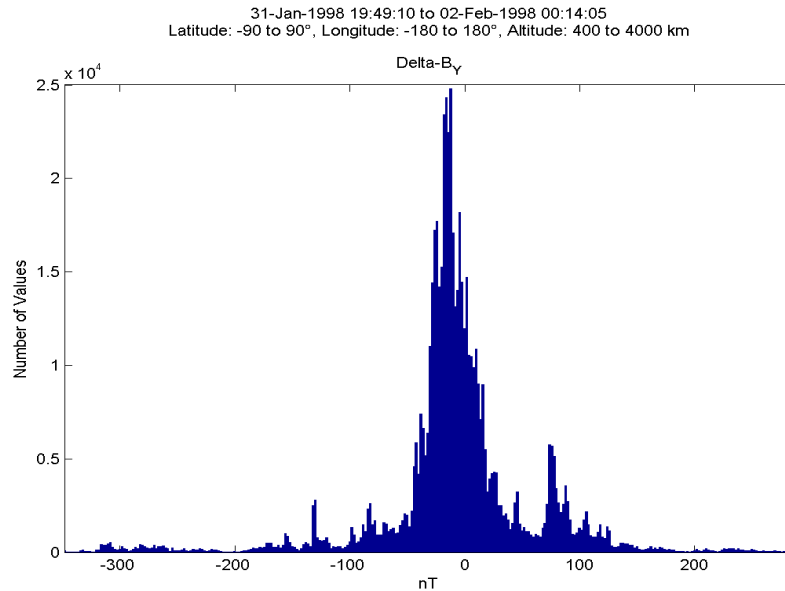


Figure 3.8: Example of Histogram

Individual orbits that have a large occurrence of values tending to not follow the normal trend of their respective binned histogram models have a higher likelihood of being considered an outlier orbit. These orbits can then be omitted from the final average Poynting and kinetic energy flux calculations.

Coordinate System Transformations

The data was exported from the SDT in one of three coordinate systems: Geocentric Equatorial Inertial Coordinate System (GEI), Data Coordinate System 2 (DCS2), or Equatorial Coordinate System (ECS). To allow for the interpretation of the calculated Poynting and kinetic energy flux with respect to the Earth, all six data types were converted into the Geocentric Coordinate System

(GEO). For more information on these coordinate systems please refer to Section 2.5 of this report. Table 3.1 shows the breakdown of the coordinate systems for each data type.

Data Type	Coordinate System
Positional	GEI
Magnetic Field	GEI
Electric Field	DCS2
Spin Axis	ECS
Electron Energy Flux	GEO
Ion Energy Flux	GEO

Table 3.1: Data Types and Their Respective Coordinate Systems

Based on Table 3.1, there were three main transformations that needed to be completed: GEI to GEO, ECS to GEO, and DCS2 to GEO.

GEI to GEO The 2010 MQP was able to develop a MATLAB function, which completed the transformation between GEI and GEO. However, based on the results of several tests, it was concluded that this function could not be used reliably. An alternative was found: Onera, the French Aerospace Lab, provides an open source MATLAB library package that was able to complete the transformation from GEI to GEO coordinates [26].

ECS to GEO As described in Section 2.5, the ECS coordinate system is composed of two angles which represent the spherical version of the GEI coordinate system. Trigonometric identities seen in equations (3.1) to (3.3) were used to convert from ECS to GEI, where RA represents the right ascension angle and D represents the declination angle of the FAST satellite.

$$x_{gei} = \sin RA \cos D \quad (3.1)$$

$$y_{gei} = \cos RA \cos D \quad (3.2)$$

$$z_{gei} = \sin D \quad (3.3)$$

Onera libraries were used to convert from the newly determined GEI coordinates to the GEO coordinate system.

DCS2 to GEO Conversion from DCS2 to GEO coordinates required the calculation of the projection of the magnetic field onto the spin plane (spB) and the perpendicular projection of the magnetic field onto the spin plane (spBp). Equations (3.4) and (3.6) show the required calculations where \mathbf{B} is the model magnetic field (IGRF) in the GEO coordinate system.

$$\hat{x}_{dcs2} = spBp = norm(spinaxis_{geoxyz} \times \mathbf{B}_{geoxyz}) \quad (3.4)$$

$$\hat{y}_{dcs2} = norm(spinaxis_{geoxyz}) \quad (3.5)$$

$$\hat{z}_{dcs2} = spB = norm(spBp \times spinaxis_{geoxyz}) \quad (3.6)$$

The projection of the magnetic field onto the spin plane (\hat{z}_{dcs2}) serves as the normalized DCS2 Z-axis vector. The perpendicular projection of the magnetic field onto the spin plane (\hat{x}_{dcs2}) serves as the normalized DCS2 X-axis vector, and the normalized spin axis vector serves as the normalized DCS2 Y-axis vector. By multiplying the X-axis in DCS2 by the X-axis represented in GEO, the Y-axis in DCS2 by the Y-axis represented in GEO, and the Z-axis in DCS2 by the Z-axis represented in GEO, individual GEO coordinate components are obtained (as seen in equations 3.7 to 3.9).

$$A_{xyz} = (x_{dcs2})(\hat{x}_{dcs2}) \quad (3.7)$$

$$B_{xyz} = (y_{dcs2})(\hat{y}_{dcs2}) \quad (3.8)$$

$$C_{xyz} = (z_{dcs2})(\hat{z}_{dcs2}) \quad (3.9)$$

The X-axis in GEO coordinates is equal to the sum of the X components of each of the previous multiplications (equation (3.10)), the Y-axis in GEO coordinates is equal to the sum of the Y components of each of the previous multiplications (equation (3.11)), and the Z-axis in GEO coordinates is equal to the sum of the Z components of each of the previous multiplications (equation (3.12)).

$$x_{geo} = A_x + B_x + C_x \quad (3.10)$$

$$y_{geo} = A_y + B_y + C_y \quad (3.11)$$

$$z_{geo} = A_z + B_z + C_z \quad (3.12)$$

Correlation of Data Time Ranges and Resolutions

Due to the sampling rate variability of the instruments on-board the FAST satellite, the data collected was not recorded uniformly. In addition, samples of the various data types were often only recorded when an interesting event took place or in only the Northern or Southern hemisphere (approximately $\pm 65^\circ$ to $\pm 90^\circ$ latitude). Therefore, the six data types collected for each orbit were recorded at different sampling resolutions over different time periods.

Table 3.2 outlines the data types used in the Poynting flux and kinetic energy flux calculations.

Poynting Flux Data Types	Kinetic Energy Flux Data Types
Positional	Positional
Magnetic Field	Electron Energy Flux
Electric Field	Ion Energy Flux
Spin Axis	

Table 3.2: Data Types Used in the Poynting and Kinetic Energy Flux Calculations

As seen in Table 3.2, the magnetic field, electric field, and spin axis data are used exclusively for the Poynting flux calculation. Furthermore, the electron and ion energy flux data are used

exclusively for the kinetic energy flux calculation; however, the positional data is used in both calculations. To account for this, two copies of the positional data were made: one to be unified to the time range and resolution of the Poynting flux data types, and one to be unified to the time range and resolution of the kinetic energy flux data types.

To resolve the time range differences between the data types used in both the Poynting and kinetic energy flux calculations, the data for one orbit was limited down to the shortest time span of the recorded data for that orbit. This was done separately for the data used in both the Poynting and kinetic energy flux calculations. If any of the data types for a single orbit were not recorded in a time span that overlapped with the time spans of the other data types, then that orbit was rejected as invalid and was not processed.

To match the resolutions of the data used in the Poynting flux calculation, the magnetic and electric field data were first passed through the single signal outlier removal function described previously, then smoothed and down-sampled to their common lowest resolution (typically the resolution of the magnetic field). The two data types were then interpolated to ensure that both sets of data had matching time columns. The spin axis and positional data used in the Poynting flux calculation were then interpolated up to the common resolution of the magnetic and electric field data. Interpolating data up to a higher resolution was used sparingly to avoid creating artificial data. However, because both the spin axis and positional data followed defined trends, accurate interpolation was possible.

The electron and ion data were recorded by the same instrument on the FAST satellite and were therefore sampled at the same rate. As a result, to match the resolutions of the data used in the kinetic energy flux calculations, the positional data was simply interpolated to the resolution of the electron and ion data.

Figure 3.9 shows a mock example of the results of matching the time ranges and resolutions of the data used in both the Poynting and kinetic energy flux calculations.

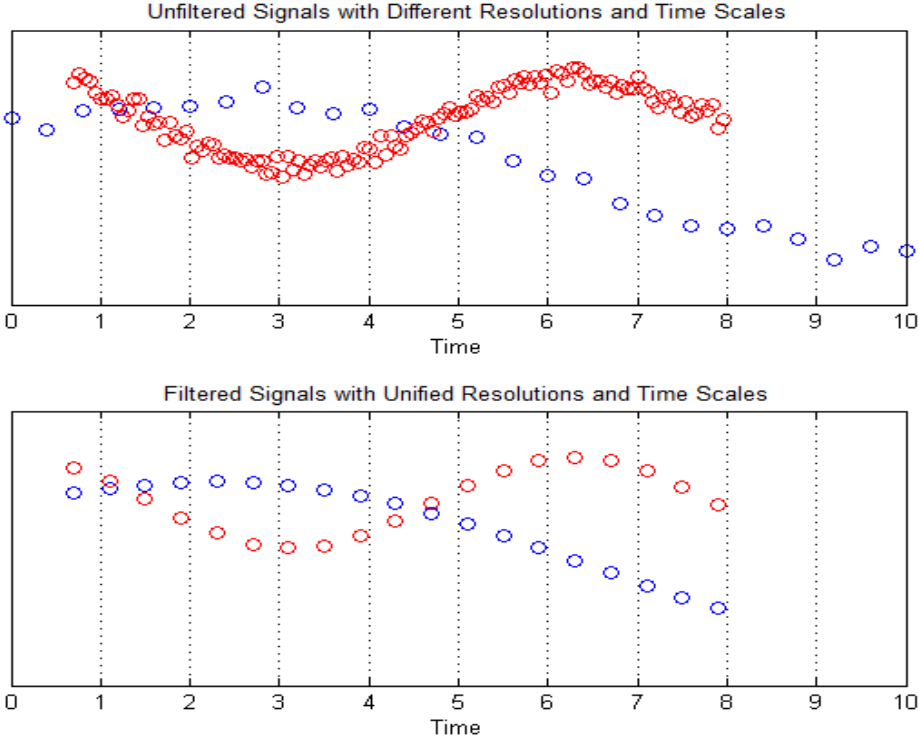


Figure 3.9: Example of Time Range and Resolution Unification of Data Types

3.1.3 Calculate the Missing Electric Field Component

Due to a malfunctioning sensor the FAST satellite was unable to collect electric field data along its spin plane axis (Y-axis DCS2). In addition, the data recorded for the electric field component along the magnetic field (Z-axis DCS2) was heavily corrupted by noise; however, through a series of calculations it is possible to determine a noise floor level that could be used to regain use of the noisy signal and approximate a reasonable value for the missing component.

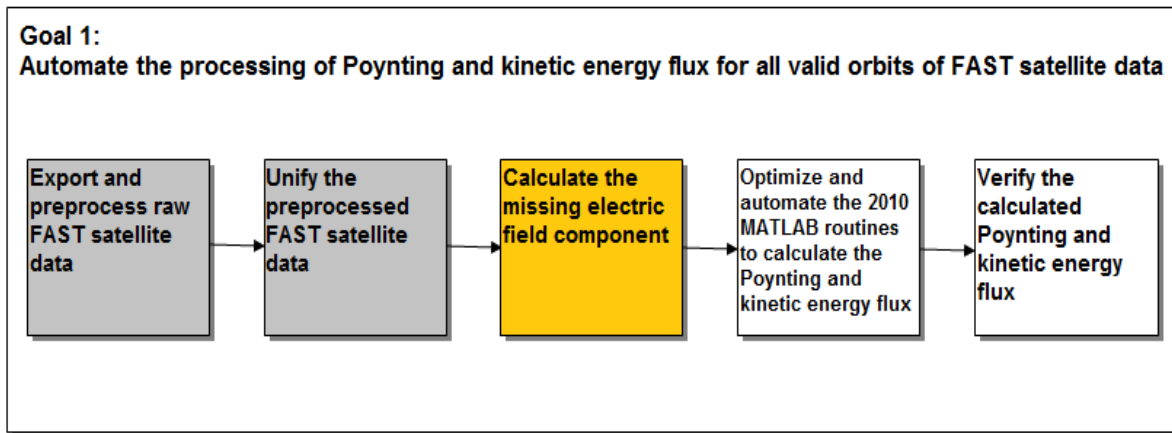


Figure 3.10: Goal 1 Block Diagram, Step 3

The process of approximating a value for the missing electric field component was split into several steps:

1. Subtract the Electric Current Generated by the FAST Satellite
2. Calculate the Angle between the Magnetic Field and Spin Plane Projection
3. Determine the Noise Floor Level in the Z Component of the Electric Field (DCS2)
4. Approximate Values for the Missing Electric Field Component

Based on the analysis of several sets of noise floor data it was observed that the noise floor level for all FAST orbits did not remain consistent. Without a confirmed noise floor level for all FAST orbits, the noise could not be eliminated from the noisy signal and an approximate value for the missing component could not be developed. However, it was determined through testing that the DCS2 Y-axis did not greatly affect the final Poynting flux calculation, and was therefore set to zero for all calculations contributing to the final binned statistical models.

The methods for approximating the value of the missing electric field component detailed below can be used for further research in future years of this project.

Subtract the Electric Current Generated by the FAST Satellite

According to Dr. Russell Cosgrove, the generated electric current offsets vary by the magnitude of the angle between the magnetic field and the spin plane. Therefore, the offsets must be subtracted from the electric field components in order to find the noise floor.

Much like how an electric current going through a loop can induce a magnetic field (Figure 3.11), a magnetic field can induce an electric current through a moving body.

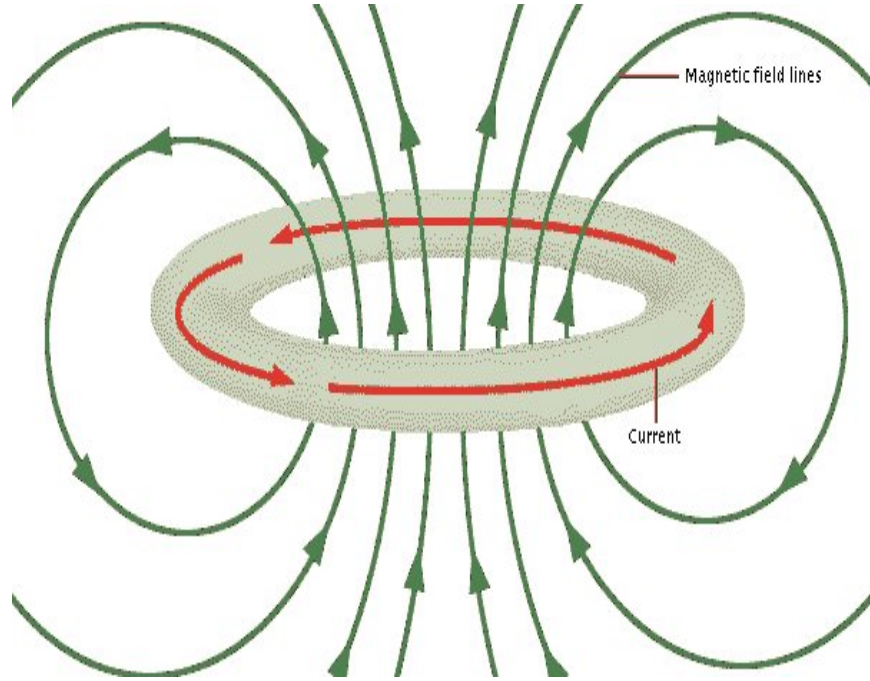


Figure 3.11: A Generated Electric Current [27]

As the FAST satellite moved across the Earth's magnetic field it produced an electric current—defined by the Lorentz Force Law, which created an offset in the data collected by the electric field sensors. This value was subtracted from the actual electric field measurement obtained from the preprocessed data. Detailed below are the steps to obtain the $V \times B$ contribution.

Calculation of the \hat{z} and \hat{x} components of the magnetic field in the DCS2 coordinate system were completed using equations (3.13) to (3.14):

$$\hat{z}_{dcs2} = norm(B_{geo_{xyz}} - (B_{geo_{xyz}} \cdot spinaxis_{geo_{xyz}}) * spinaxis_{geo_{xyz}}) \quad (3.13)$$

$$\hat{x}_{dcs2} = norm(spinaxis_{geo_{xyz}} \times \hat{z}_{dcs2}) \quad (3.14)$$

The external electric field contribution can be found by taking the dot product of the previous two equations (3.13 and 3.14) with the cross product of the velocity and model magnetic field (IGRF):

$$E_{z_{V \times B}} = -(V_{geo_{xyz}} \times (B_{geo_{xyz}}) \cdot \hat{z}_{dcs2}) \quad (3.15)$$

Similarly for $E_{x_{V \times B}}$:

$$E_{x_{V \times B}} = -(V_{geo_{xyz}} \times (B_{geo_{xyz}}) \cdot \hat{x}_{dcs2}) \quad (3.16)$$

The new calculated E_{dcs2_z} and E_{dcs2_x} components of the electric field can be determined by subtracting these offsets:

$$E_{dcs2_z} = E_{dcs2_z} - E_{z_{V \times B}} \quad (3.17)$$

$$E_{dcs2_x} = E_{dcs2_x} - E_{x_{V \times B}} \quad (3.18)$$

An example of the $V \times B$ contribution with its respective electric field can be seen in Figure 3.12. Correcting the electric field measurements enables calculation of downward Poynting flux measurements pertaining only to atmospheric effects.

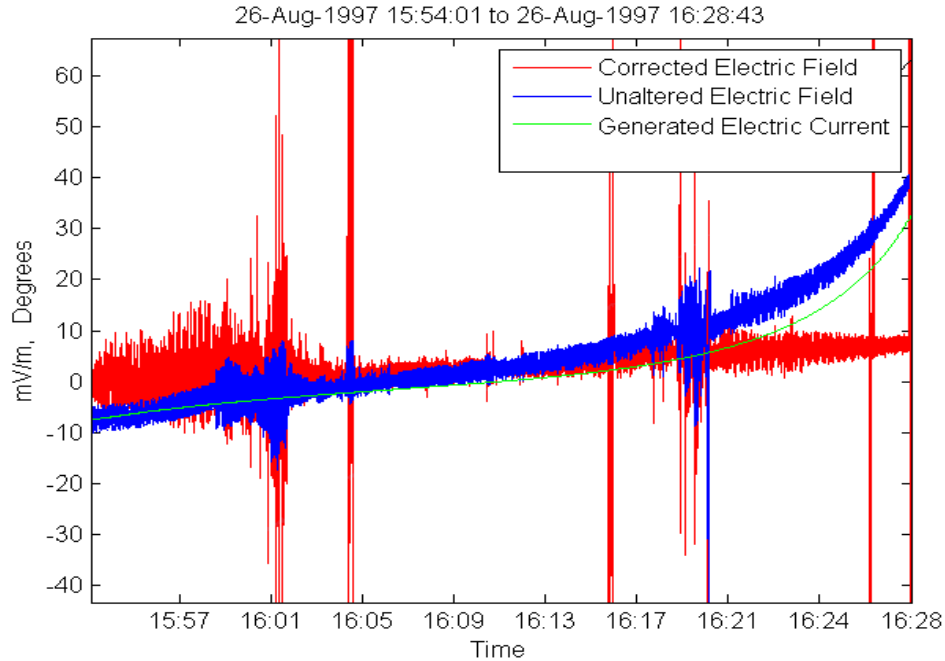


Figure 3.12: Observed Generated Electric Current Offset

Calculate the Angle between the Magnetic Field and Spin Plane Projection

Using the original Poynting flux calculations used by the 2010 MQP, the Y-axis and Z-axis of the electric field components were set to zero. Due to the variability in the magnetic field across the orbital path of the satellite, the angle between the magnetic field and the projection of the magnetic field onto the satellite's spin plane changes over time.

As the angle increases, the X-axis electric field component more accurately represents the total electric field. Therefore a smaller angle creates a larger error in the final Poynting flux results calculated when using the original 2010 MQP calculations whereby the Y-axis and Z-axis of the electric field are set to zero.

The angle between the magnetic field and the projection of the magnetic field onto the satellite's spin plane is calculated using equation (3.19). The calculated value θ is the angle between the magnetic field and the projection of the magnetic field, \mathbf{B} is the model magnetic field (IGRF), and \hat{z}_{dcs2} , calculated in equation (3.13), is the projection of the magnetic field onto the satellite's spin plane.

$$\theta = 90 - \arccos(\mathbf{B} \times \hat{z}_{dcs2}) \quad (3.19)$$

Determine the Noise Floor Level in the Z Component of the Electric Field (DCS2)

After successfully removing the generated electric current ($V \times B$ contribution) from the electric field data, it was possible to create binned plots using the calculated angle between the magnetic field and the spin plane projection. By plotting the Z component of the electric field data against θ (equation 3.19), models were created which were used to determine the threshold at which the Z-axis of the electric field data was unaffected by noise and was therefore considered usable. Those electric field values that fell beneath the value of the noise floor level would be rejected.

Each generated model was a plot of the root mean squared value of all electric field data within a 0.01° range of the angle between the magnetic field and its spin plane projection known as θ . The overall angle range was set between $\pm 20^\circ$ to include all calculated values of the angle.

Data from various orbit ranges were used to determine the noise floor. Figures 3.13 and 3.14 show the binned empirical models created for two different ranges of FAST satellite orbits. Figure 3.13 indicates a noise floor level of approximately 3 mV/m while Figure 3.14 indicates a noise floor level of approximately 8 mV/m.

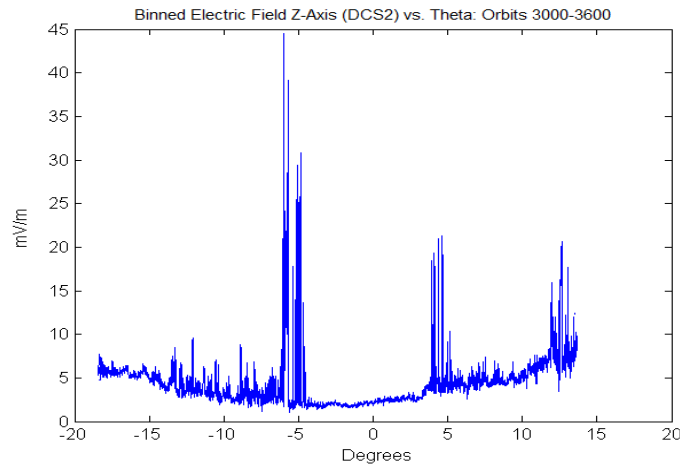


Figure 3.13: Noise Floor Level for Orbits 3000-3600: Approximately 3 mV/m

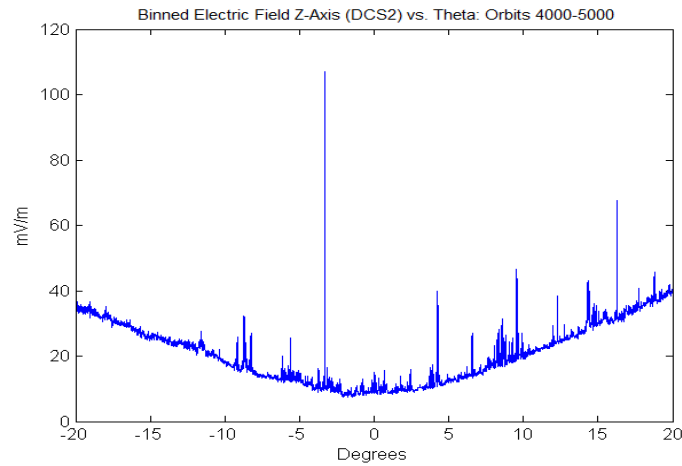


Figure 3.14: Noise Floor Level for Orbits 4000-5000: Approximately 8 mV/m

Approximate Values for the Missing Electric Field Component

As described, due to the variability in the noise floor level a method for calculating the appropriate noise floor level for all FAST orbits was necessary. Due to the limited time frame of this project, such a method was never fully developed and thus the electric field data for the Y-axis was not recovered. However, for future projects attempting to calculate an appropriate noise floor level for all FAST orbits, the previous sections can be used to aid in the approximation of the missing electric field component.

3.1.4 Optimize and Automate the 2010 MATLAB Routines to Calculate the Poynting and Kinetic Energy Flux

The 2010 MQP was focused on developing MATLAB routines that could calculate the Poynting and kinetic energy flux for a given individual orbit of the FAST satellite. Working off of these routines, optimized routines that were able to complete these calculations for approximately 20,000 orbits worth of valid FAST data were developed.

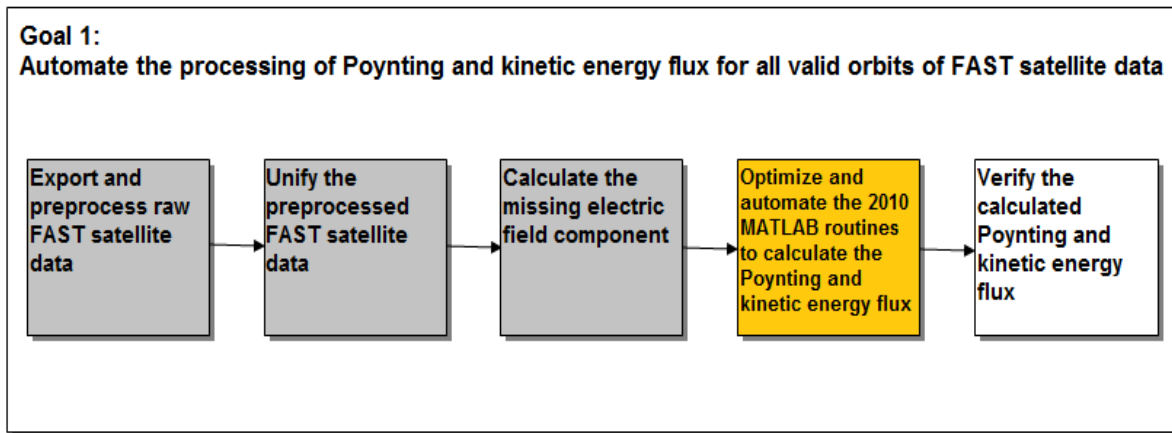


Figure 3.15: Goal 1 Block Diagram, Step 4

Additionally, these optimized routines were tailored to work with the unified FAST data developed through methods described in Section 3.1.2.

Described in Appendix A.2, the Poynting flux was calculated by taking the cross product of the unified electric field and $\delta\mathbf{B}$ data, and dividing by the permeability of free space (equation (2.1)). To obtain the Poynting flux data mapped down the magnetic field, the final Poynting flux values calculated from data recorded in the Southern hemisphere were negated. For each valid FAST orbit, the Poynting flux was calculated in both GEI and GEO coordinate systems and saved to two separate MATLAB files. These files were stored onto a hard drive in a folder labeled “Processed Data”. This folder contained already processed Poynting flux calculations which made it faster for plotting using the “histograms” and “3D Polar Plots” functions. At the end of this year’s project, the hard drive was given to Dr. Russell Cosgrove and Dr. Hasan Bahcivan to use in the future years of this project.

The electron and ion files that were exported from IDL and unified in MATLAB contained the ion and electron energy flux mapped to an altitude of 100 km. By taking the summation of these two parameters the kinetic energy flux could be determined. Although the data required for the calculations of the kinetic energy flux were unified in the final MATLAB routines, due to time limitations the final kinetic energy results were not completed.

To allow for the future accurate analysis of the Poynting flux data with the kinetic energy flux data, the Poynting flux results were mapped to an altitude of 100 km. To complete the mapping

the Poynting flux results were multiplied by the ratio of the magnetic field mapped to 100 km and the unmapped magnetic field. Both the mapped and unmapped magnetic fields were parameters that were exported directly from the SDT and IDL routines.

3.1.5 Verify the Calculated Poynting Flux

Before developing the binned statistical visual models of the Poynting flux values developed in the previous steps of Goal 1, the calculated Poynting flux values had to be verified.

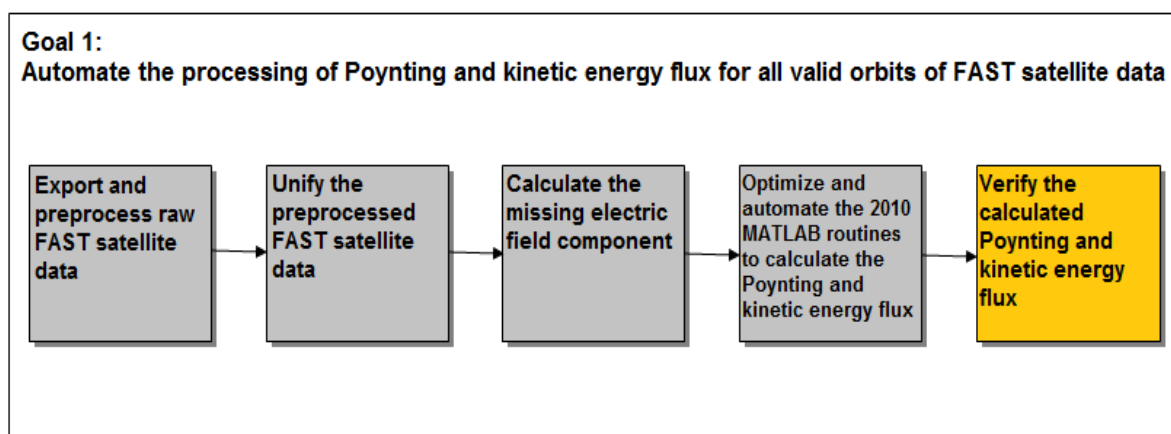


Figure 3.16: Goal 1 Block Diagram, Step 5

To verify the calculated Poynting flux, the values were compared against data recorded by radar located at the Sondrestrom Research Facility in Kangerlussuaq, Greenland. The comparisons were made using Poynting flux data calculated from measurements recorded by the FAST satellite while it was within $\pm 1^\circ$ latitude and $\pm 2.5^\circ$ longitude of the Sondrestrom Research Facility. Over the 20,000 valid FAST orbits, there were approximately 200 incidents of FAST satellite recording data within the appropriate latitude and longitude range. Of these 200 incidents, there were only approximately twenty overlaps of time when the radar was also recording data.

The majority of the comparisons made revealed measured magnitudes that were too small to be used for accurate verification. Based on the limited number of viable comparisons, it was determined that although the Poynting flux values have not been verified, the results look promising and should be investigated further in future years of this project.

3.2 Develop Binned Statistical Visual Models

Interpretation of the calculated Poynting and kinetic energy flux still needed to be accomplished; however, data interpretation is better done through the use of visual models, such as plots. The second goal of this project aimed to create such visual tools that would aid researchers in better understanding the previously calculated data.

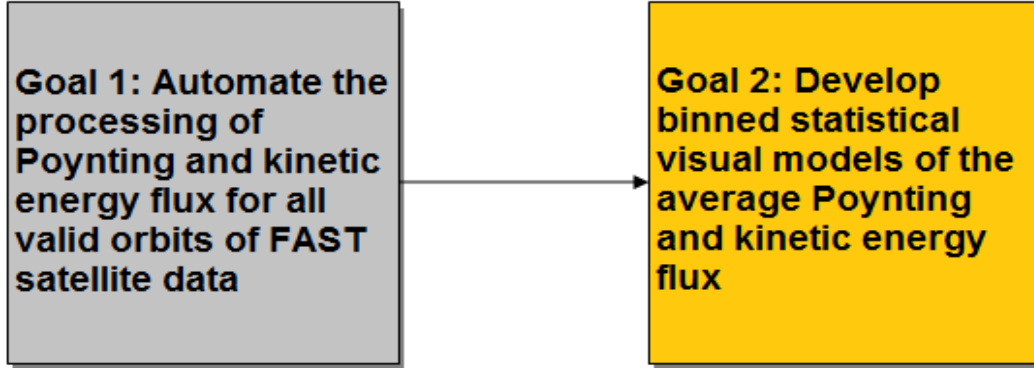


Figure 3.17: Goal 2 Block Diagram

3.2.1 3D Polar Plots

In order to understand the various effects of Poynting flux visual interpretation was required. The function “POLAR3D.m”, written by J. M. De Freitas, was used in order to create the 3D polar plot of the binned statistical Poynting flux average [28]. This function was available for public use on the MATLAB Exchange by The Mathworks, Inc. The geophysical parameters (altitude, ap index, invariant latitude, and magnetic local time) were used to bin the data. Based on these geophysical parameters the Poynting fluxes that fell within the range were binned appropriately using a weighted average scheme. A function was created that would be able to find the average Poynting fluxes that fell within each bin and weight it based on the number of occurrences:

$$S_{total_{avg}} = \frac{S_{avg_1}N_1 + S_{avg_2}N_2 \dots + S_{avg_n}N_n}{N_1N_2 \dots N_n} \quad (3.20)$$

Where n is equal to the number of orbits that fell within a certain bin, S was the average of the Poynting fluxes of an individual orbit that fell within a certain bin, and N was equal to the

number of points in each orbit that fell within a certain bin. This was calculated for each bin of the polar plot function to create a mass binned statistical model.

Chapter 4

Results

The main goal of this project was to develop MATLAB routines that automatically created binned statistical models of the average Poynting flux based on several geophysical parameters. The binned statistical models created were in the form of polar plots, which displayed average Poynting flux values plotted against magnetic local time and invariant latitude. The magnetic local time is displayed around the circumference of the plot and the invariant latitude is displayed along the radius of the plot. Figures 4.1 and 4.2 are examples of the polar plots that were created.

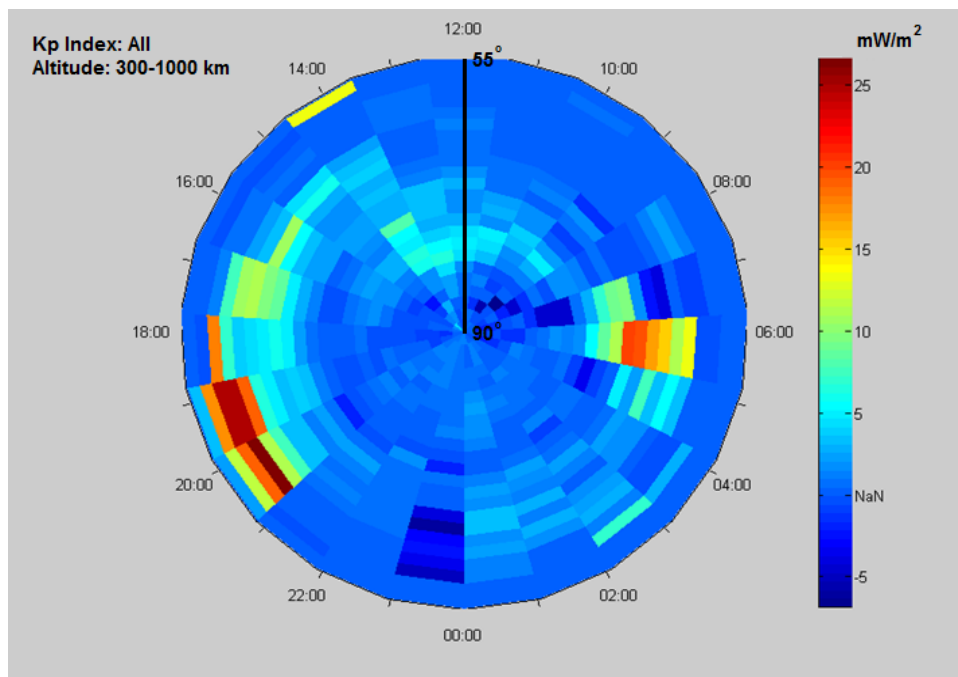


Figure 4.1: Average Poynting Flux in the Northern Hemisphere

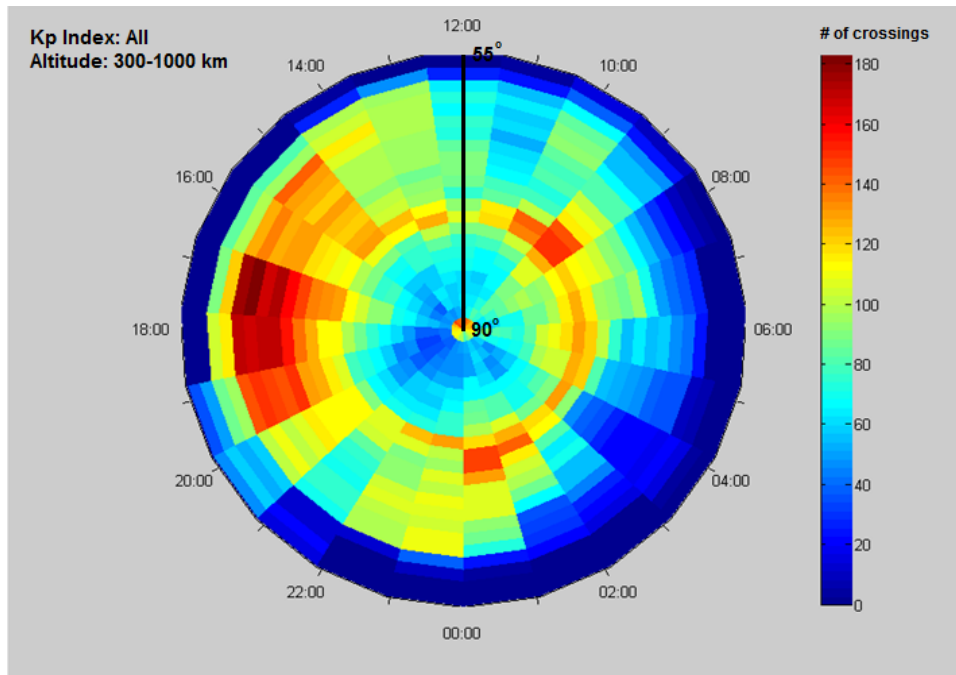


Figure 4.2: Contributing Crossings to the Average Poynting Flux in the Northern Hemisphere

Figure 4.1 is a polar plot of the average Poynting flux from 55° to 90° invariant latitude, 300-1000 km altitude, and all ap index values. This plot is created using approximately 3,000 orbits worth of FAST satellite data collected over a time period of 15 months. Figure 4.2 is a plot of the number of FAST orbital crossings that contributed to the average Poynting flux values displayed in Figure 4.1. Crossings plots (Figure 4.2) can be used for more accurate analysis of the average Poynting flux values calculated. The greater the number of contributing crossings for a certain segment of Poynting flux intensity, the greater the validity of that data due to more orbits contributing to the average calculated Poynting flux. For example, in Figure 4.1 the high Poynting flux intensity recorded at 55° , 14:00 MLT has very few contributing crossings as seen in Figure 4.2. Therefore, this value is likely an outlier value and can be disregarded.

The highest instances of Poynting flux intensity in Figure 4.1 occur at approximately 6:00 and 18:00 MLT as the Sun is rising and setting. The latitude values for both instances occur between approximately 60° and 70° invariant latitude, which fall within the latitude range of the auroral acceleration region. Based on this preliminary analysis, the generated plots indicated reasonable instances of high Poynting flux intensity.

To verify the results obtained, comparisons against preexisting statistical models were made. Figure 4.3 shows a side-by-side comparison of the polar plot presented in Figure 4.1 against a polar plot presented by Deng et al. in an article published in the Journal of Geophysical Research [29].

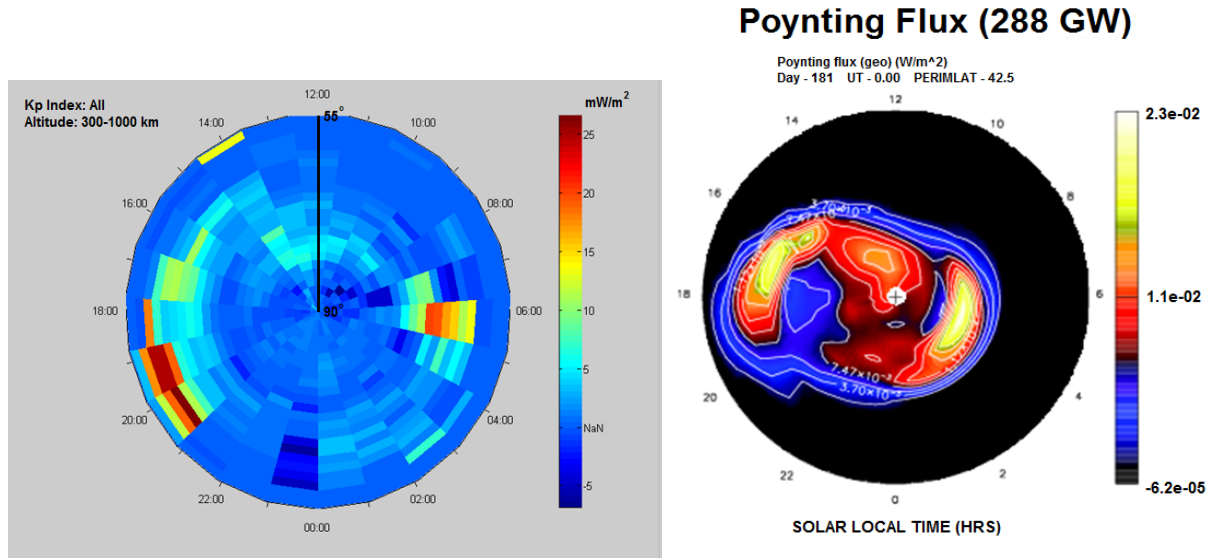


Figure 4.3: Verification of Calculated Average Poynting Flux [29]

In both plots the highest instances of Poynting flux occur at comparable latitude ranges at approximately 60° and 70° . Both plots were created using data collected at comparable altitudes (1000 km for Deng et al.) and over all Kp index values. Figure 4.3 does not provide a direct comparison. The Deng et al. model is plotted against solar magnetic time, not magnetic local time; however at lower altitudes the solar magnetic time is relatively similar to that of magnetic local time. The Deng et al. model also represents data recorded over only the summer season, compared to all seasons represented in the model produced as a result of this project – this comparison does indicate that the results obtained look very promising and should be investigated further in future years of this project.

Chapter 5

Recommendations

During the completion of this project, areas of research were unable to be addressed due to time limitations. As such, it is recommended that the 2012 MQP group continue from where the 2011 MQP group left off.

- Verify the validity of all re-preprocessed data for each orbit. It is advised that they should verify all data files for each orbit and remove those orbits whose data is deemed invalid. Alternatively they could work to develop error checking algorithms that will accurately eliminate outlier orbits. While a significant amount of outliers were removed in each data set – in addition to rejecting all orbits that did not have available data for all six files – there is still reason to believe that there may be some invalid data that was not eliminated from the binned statistical models.
- Adjusting the existing electric field processing code work with user inputted altitude ranges. Near the end of the project, Dr. Bahcivan and Dr. Cosgrove expressed interest in analyzing altitude specific electric field binned data in order to obtain more precise data plots for specified regions of the atmosphere. Unfortunately, there was not enough time left in the project at the time of its suggestion and as such the task was not met.
- Further investigation into the validity of the newly preprocessed and exported magnetic and electric field data sets. Confirmation was sought with Dr. Strangeway from the University of California, Los Angeles but due to the time limitations a consensus was not reached.
- Recalculate the electric field noise floor and ensure it's validity. Upon doing so attempt to recover the missing electric field component.

Chapter 6

Conclusion

This project was the second iteration of a four year research endeavor proposed by SRI International and funded by the National Science Foundation (NSF). The purpose of this year's project was to automate the process of calculating and developing binned statistical visual models of the average downward Poynting and kinetic energy flux as recorded by the Fast Auroral SnapshoT (FAST) satellite. These models will ultimately serve to further the understanding of the Sun's energy input into Earth's thermosphere.

Continuing on the progress made by the 2010 MQP, this project worked to accomplish two main goals:

1. Automate the Poynting and kinetic energy flux processing of the FAST satellite data.
2. Develop binned statistical visual models (i.e. polar plots) of the Poynting flux and kinetic energy flux data recorded by the FAST satellite.

To accomplish the first goal of this project, Interactive Data Language routines were used to re-preprocess approximately 20,000 orbits of FAST satellite data from remote servers at the University of California, Berkeley. The preprocessed data was exported into six separate Common Data Format (CDF) files per orbit and saved to a single directory stored on an external hard drive. Each CDF file contained a different data type that was used in calculating the Poynting and kinetic energy flux. MATLAB routines were created to unify the preprocessed data by completing outlier removal, coordinate system transformations, and matching the time ranges and resolutions of the different data types used in both the Poynting and kinetic energy flux calculations. Although the data for the calculation was prepared, due to time limitations the kinetic energy flux was not

calculated as a part of this project. However, MATLAB routines to automatically and efficiently calculate the Poynting flux for all valid orbits of unified FAST data were successfully developed.

Using the calculated Poynting flux results obtained in completion of the first goal, MATLAB functions were developed that automatically create binned statistical visual models of the average Poynting flux over a given range of geophysical parameters. The statistical models were compared against preexisting statistical models published by researchers Deng et al. in the Journal of Geophysical Research. Preliminary comparisons suggest that the statistical models created as a final result of this project look promising and should be further analyzed in future years of this project.

The final two years of this project will work toward developing analytical models that will serve as physical interpretations of the Sun's energy input into Earth's thermosphere. These interpretations will aid in the effort characterizing space weather effects, ultimately leading to improvements in spacecraft and communication systems design.

Appendix A

Algorithms and Calculations

A.1 Outlier Removal Algorithm

The following equations are used to figure out which data points within a sample signal may be considered outliers. Using a zero-mean Gaussian probability density function (pdf) it is known that:

$$f(y = |V|^2) = \frac{1}{2\pi\sigma^2} e^{\left(\frac{-y^2}{2\sigma^2}\right)} \quad (\text{A.1})$$

Where $|V|$ is the absolute value of the original input signal. To find the value for σ , the formula is integrated with respect to y given that $f(y = |V|^2)$ is set to be a 50% chance that a single data point will exceed the threshold. The bounds of the integral will be 0 to the median of the signal squared which will be called x . Thus equation (A.1) integrates to:

$$\int_0^x \frac{1}{2\pi\sigma^2} e^{\left(\frac{-y^2}{2\sigma^2}\right)} dy = \frac{1}{2} = -e^{\left(\frac{-y}{2\sigma^2}\right)} \Big|_0^x \quad (\text{A.2})$$

Solving for the equation (A.2) yields:

$$-e^{\left(\frac{-x}{2\sigma^2}\right)} + 1 = \frac{1}{2} \quad (\text{A.3})$$

Taking the natural log of both sides in equation (A.3):

$$\frac{x}{2\sigma^2} = \ln(2) \quad (\text{A.4})$$

Setting $x = \text{median}(|V|^2)$ the equation can be solved for the value of σ :

$$\sigma = \sqrt{\frac{\text{median}(|V|^2)}{2\ln(2)}} \quad (\text{A.5})$$

The likelihood that a window of length n data points would exceed a given threshold is given by:

$$\frac{1}{2} = 1 - (1 - \alpha)^n \quad (\text{A.6})$$

Where $\frac{1}{2}$ is set to be a 50% chance that a point will exceed the threshold. Thus α is the likelihood that at least one point out of n will exceed the threshold. Solving for α :

$$\alpha = 1 - \left(\frac{1}{2}\right)^{\frac{1}{n}} \quad (\text{A.7})$$

The variable α is now set to equal equation (A.2), except the integral from a certain threshold, which will be labeled as \mathbf{S} , to infinity, may now be solved.

$$\alpha = \int_{\mathbf{S}}^{\infty} \frac{1}{2\pi\sigma^2} e^{\left(\frac{-y^2}{2\sigma^2}\right)} dy = -e^{\left(\frac{-y}{2\sigma^2}\right)} \Big|_{\mathbf{S}}^{\infty} \quad (\text{A.8})$$

Solving for equation (A.8) we have:

$$\alpha = 0 + e^{\left(\frac{-\mathbf{S}}{2\sigma^2}\right)} = 1 - \left(\frac{1}{2}\right)^{\frac{1}{n}} \quad (\text{A.9})$$

Simplifying equation (A.9) the threshold value \mathbf{S} can be found:

$$\mathbf{S} = -2\sigma^2 \ln\left(1 - \left(\frac{1}{2}\right)^{\frac{1}{n}}\right) \quad (\text{A.10})$$

The threshold value \mathbf{S} must be calculated for each window of the signal. In order to obtain an accurate σ value, a best fit m-polynomial is fitted to the windowed curve of the signal such that values that exceeded the certain threshold \mathbf{S} on the polynomial fit would effectively be discarded.

A.2 Poynting Flux Calculations

All calculations below are matrix operations and in standard SI units, unless otherwise specified.

The spin-axis data must first be in the GEI coordinate system for any further calculations to be completed:

$$x_{gei} = \sin RA \cos D \quad (\text{A.11})$$

$$y_{gei} = \cos RA \cos D \quad (\text{A.12})$$

$$z_{gei} = \sin D \quad (\text{A.13})$$

Where RA and D are the right ascension and declination angles of the spacecraft given in ECS coordinates. Changing from GEI to GEO coordinates is a simple transformation as it relies on the Greenwich Hour Angle outlined in (Coordinate systems conversions background section).

Before any calculations for Poynting flux are made, the electric field (E) offsets contributed by $V \times B$ needed to first be calculated:

First the \hat{z}_{dcs2} component needed to be calculated:

$$\hat{z}_{dcs2} = \text{norm}(B_{geoxyz} - (B_{geoxyz} \cdot \text{spinaxis}_{geoxyz}) * \text{spinaxis}_{geoxyz}) \quad (\text{A.14})$$

Where B_{geoxyz} is the model B field (IGRF), spinaxis_{geoxyz} is the calculated spin-axis from the right ascension and declination angles of the spacecraft. Then the \hat{x}_{dcs2} offset is found to be:

$$\hat{x}_{dcs2} = \text{norm}(\text{spinaxis}_{geoxyz} \times \hat{z}_{dcs2}) \quad (\text{A.15})$$

Thus to find the $V \times B$ contribution of each component (row wise operation to create a single column matrix):

$$E_{z_{V \times B}} = -((V_{geoxyz} \times B_{geoxyz}) \cdot \hat{z}_{dcs2}) \quad (\text{A.16})$$

Similarly for $E_{x_{V \times B}}$:

$$E_{x_{V \times B}} = -((V_{geoxyz} \times B_{geoxyz}) \cdot \hat{x}_{dcs2}) \quad (\text{A.17})$$

Where $V_{geo_{xyz}}$ is the velocity of the spacecraft in GEO coordinates. The new calculated E_{dcs2_z} and E_{dcs2_x} components of the electric field can be determined by subtracting these offsets:

$$E_{dcs2_z} = E_{dcs2_z} - E_{z_{V \times B}} \quad (\text{A.18})$$

$$E_{dcs2_x} = E_{dcs2_x} - E_{x_{V \times B}} \quad (\text{A.19})$$

Once the electric field offsets are corrected, transformation from the DCS2 coordinate system to GEO coordinate system is necessary. It is determined that the DCS2 unit vector components are:

$$\hat{x}_{dcs2} = spBp = norm(spinaxis_{geo_{xyz}} \times B_{geo_{xyz}}) \quad (\text{A.20})$$

$$\hat{y}_{dcs2} = norm(spinaxis_{geo_{xyz}}) \quad (\text{A.21})$$

$$\hat{z}_{dcs2} = spB = norm(\hat{x}_{dcs2} \times spinaxis_{geo_{xyz}}) \quad (\text{A.22})$$

Where spB is the spin plane projection of the magnetic field (B) and $spBp$ is the perpendicular spin plane projection of the magnetic field (B). Now multiplying each by actual DCS2 values:

$$A_{xyz} = \hat{x}_{dcs2} * E_{dcs2_x} \quad (\text{A.23})$$

$$B_{xyz} = \hat{y}_{dcs2} * E_{dcs2_y} \quad (\text{A.24})$$

$$C_{xyz} = \hat{z}_{dcs2} * E_{dcs2_z} \quad (\text{A.25})$$

Taking each x, y, and z components creates the GEO coordinate components of the electric field:

$$E_{geo_x} = A_x + B_x + C_x \quad (\text{A.26})$$

$$E_{geo_y} = A_y + B_y + C_y \quad (\text{A.27})$$

$$E_{geo_z} = A_z + B_z + C_z \quad (\text{A.28})$$

Now that the electric field data is in GEO coordinates, calculation of the Poynting flux can be done. When the satellite is in the northern hemisphere the Poynting flux (S) is calculated as:

$$S = \frac{(E_{geo} \times \delta B_{geo}) \cdot \hat{B}_{geo_{xyz}}}{\mu_0} \quad (\text{A.29})$$

Where δB_{geo} is the perturbation caused by the difference between the model and measured magnetic field and $\hat{B}_{geo_{xyz}}$ is the normalized unit vector of the model magnetic field. When the satellite is in the southern hemisphere the equation to calculate the Poynting flux is:

$$S = \frac{-(E_{geo} \times \delta B_{geo}) \cdot \hat{B}_{geo_{xyz}}}{\mu_0} \quad (\text{A.30})$$

It is multiplied by a negative to make the Poynting flux point downwards towards Earth. Then taking into account that the electron and ion data is mapped to 100 km, the Poynting flux also needs to be mapped to that reference altitude for comparisons. This is done by taking the ratio of the magnetic field at 100 km and at the reference altitude of the data point (ALT):

$$S_{100km} = \frac{\hat{B}_{100km}}{\hat{B}_{ALT}} S_{ALT} \quad (\text{A.31})$$

Appendix B

Authorship and Deliverables

B.1 Authorship

The primary authors of each section of this report are outlined below. All sections were edited by all three partners of this project.

1. Abstract - Author: Steven Chen
2. Executive Summary - Author: Steven Chen
3. Acknowledgments - Author: James Rehberger
4. Introduction - Author: Steven Chen
5. Background
 - (a) Earth's Atmosphere - Author: James Rehberger
 - (b) Space Weather and its Effects on Earth - Author: Megan Van Welie
 - (c) Fast Auroral SnapshoT Satellite - Author: Steven Chen
 - (d) Accessing FAST Satellite Data - Author: Steven Chen
 - (e) Coordinate Systems Represented by the FAST Data - Author: James Rehberger
 - (f) Poynting and Kinetic Energy Flux - Author: Steven Chen
 - (g) Geophysical Parameters - Author: Megan Van Welie
6. Methodology and Implementation
 - (a) Automating the Processing of Poynting and Kinetic Energy Flux

- i. Export and Preprocess Raw FAST Satellite Data - Author: Steven Chen
 - ii. Unify the Preprocessed FAST Satellite Data - Author: Megan Van Welie
 - iii. Calculate the Missing Electric Field Component - Author: James Rehberger
 - iv. Optimize and Automate the 2010 MATLAB Routines to Calculate the Poynting and Kinetic Energy Flux - Author: Megan Van Welie
 - v. Verify the Calculated Poynting and Kinetic Energy Flux - Author: Megan Van Welie
- (b) Developing Plots and Binned Statistical Models
- i. 3D Polar Plots - Author: Steven Chen
7. Results - Author: Megan Van Welie
8. Recommendations - Author: James Rehberger
9. Conclusion - Author: Megan Van Welie
10. Appendix A
- (a) Outlier Removal Algorithm - Author: Steven Chen
 - (b) Poynting Flux Calculations - Author: Steven Chen
11. Appendix B
- (a) Authorship - Author: Megan Van Welie
 - (b) Deliverables - Author: Megan Van Welie

B.2 Deliverables

This appendix outlines the primary authors of all deliverables presented to Dr. Russell Cosgrove and Dr. Hasan Bahcivan at the conclusion of this project. Future years of this project may contact the respective authors of each deliverable for additional information and troubleshooting help. Steven Chen may be contacted at googly.bear@gmail.com, Megan Van Welie may be contacted at megan6459@gmail.com, and James Rehberger may be contacted at jrehberger@wpi.edu.

IDL Routines

- `make_efields_cdf.pro` - Edited by: Steven Chen
- `make_orbit_cdf.pro` - Edited by: Steven Chen
- `get_fa_attidue.pro` - Edited by: Steven Chen
- `make_all_cdf.pro` - Author: Steven Chen
- `batch_processing.pro` - Author: Steven Chen
- `timeout.pro` - Author: Steven Chen

MATLAB Routines

- `bin_mass.m` - Author: James Rehberger
- `data_interp.m` - Author: Megan Van Welie
- `dcs2togeom.m` - Author: Megan Van Welie
- `down_smooth.m` - Author: Megan Van Welie, Co-Author: Steven Chen
- `ecurrent_offset.m` - Author: Megan Van Welie, Co-Author: Steven Chen
- `efield_singlebin.m` - Author: James Rehberger, Co-Author: Megan Van Welie
- `get_efield.m` - Author: Steven Chen, Co-Author: Megan Van Welie
- `get_spin_axis.m` - Author: Megan Van Welie, Co-Author: James Rehberger
- `get_theta.m` - Author: Megan Van Welie, Co-Author: James Rehberger
- `kp_to_unixtime.m` - Author: Steven Chen
- `limit_check.m` - Author: Megan Van Welie
- `limit_kp.m` - Author: Steven Chen
- `load_data.m` - Author: Megan Van Welie
- `mat2unixtime.m` - Author: Steven Chen

- orbit_stats.m - Author: Megan Van Welie
- orbit_stats_plots.m - Author: Megan Van Welie
- outlier_removal.m - Author: Steven Chen
- plot_individual_orbits.m - Author: Megan Van Welie
- polar_plot.m - Author: Megan Van Welie, Co-Author: Steven Chen
- polar3d.m - Edited by: Megan Van Welie
- process_flux.m - Author: Megan Van Welie
- process_orbit.m - Author: Steven Chen
- radar_locate.m - Author: Megan Van Welie
- radar_locate_times.m - Author: Megan Van Welie
- search_orbit.m - Author: Steven Chen
- sequential_orbit.m - Author: Steven Chen
- zin_for_polar3D.m - Author: Megan Van Welie, Co-Author: Steven Chen

Appendix C

Tutorials

C.1 SDT and IDL

Written By: Steven Chen

3/4/11

googly.bear@gmail.com

Due to unforeseen circumstances, some of the data files might not have been created. This is partly due to either invalid data, or no data being recorded for a certain DQD - "Data Quantity Descriptor". This tutorial will attempt to guide a new user through how to use SDT and IDL on-site at SRI.

*****Poynting Flux Data*****

Accessing SDT on llama:

1. Start off by starting up Xming XLaunch.
2. Select "One window" -> Next
3. Select "Open session via XDMCP" -> Next
4. Check "Connect to host" and in the empty box insert: llama.sri.com
5. Press next once more.
6. For the username input: nicole
7. For the password input: *****
8. To launch SDT, with the correct configuration files while logged in as nicole type in the terminal window:

```
llama [~]> cd fast
```

```
llama [~]> sdt &
```

(Ctrl+C in the terminal window will get you a new command prompt)

9. Select "Configuration Files" and scroll to down to find UIcfg.wpi5716, you may also create your own plots, but I suggest sticking with the one that displays all needed data.
10. Select it and click "without raw data". This will open up several plots and the SDT user interface.
11. If you want to view a certain orbit right click in an empty space not within a plot, and select DataFromNetwork.
12. Type in the orbit of interest and press "Okay".
13. Most times files will be downloaded, if so press "Download all files and plot".
14. Give the server some time to plot as they take time. The DQDs shown in the SDT user interface are all the required fields needed to process the magnetic field, electric field, spin axis angle, and the orbital data.
15. You can also run IDL routines from the terminal window. Type:

```
llama [~]> idl -32
```

```
IDL>batch_processing
```

This will automatically process all of the data relevant to the orbit selected.

The data will be stored in a different processed data directory, which is listed below (see below -unique to each server).

Other routines of interest are:

```
ucla_mag_despin
```

```
fields_despin
```

These are the routines responsible for despining the magnetic and electric field data.

16. Now to quit out of SDT, click the [-] button and close, or just simply select the window and ALT+f4.

17. Sometimes you need to make sure that SDT is actually closed, so check by issuing a command to the shell window:

```
llama [~]> env |grep sdt| more
```

(CTRL+z to suspend)

```
llama [~]>kill -9 *proccessid*
```

or just simply type in the terminal:

```
llama [~]> cleanup
```

Accessing SDT on ISR:

1. Same as steps 1-7 as above.
2. In the terminal window type:

```
llama [~]> ssh schen@isr.sri.com
```

```
Password : *****
```

3. We are now on the ISR server. Due to authentication issues the schen account does not have a valid .Xauthority cookie, so type:

```
isr [~]> cp /home/nicole/.Xauthority .
```

This will copy nicole's .Xauthority cookie allowing emacs and SDT to show up

correctly.

4. You do not need to switch directories as this account was made specifically for batch processing. So launch SDT:

```
isr [~]> sdt &
```

5. The same commands and instructions for LLAMA apply for ISR as well for usage of IDL routines.

Accessing SDT on VIPER:

1. Same as steps 1-7 as above.
2. In the terminal window type:

```
llama [~]> ssh schen@viper.sri.com
```

```
Password : *****
```

3. We are now on the VIPER server. Due to authentication issues the schen account does not have a valid .Xauthority cookie so type:

```
viper [~]> cp /home/nicole/.Xauthority .
```

This will copy nicole's .Xauthority cookie allowing emacs and SDT to show up correctly.

4. You do not need to switch directories as this account was made specifically for batch processing. So launch SDT:

```
viper [~]> sdt &
```

5. The same commands and instructions for LLAMA apply for VIPER as well for usage of IDL routines.

***** Batch Mode *****

Batch mode does not require the SDT user interface to be open in order to process the data and export it.

Running `sdt_batch` requires you to be in the home folder.

```
>cd $HOME
```

Once there type:

```
>sdt_batch sdt_test.batch
```

Where the test batch is the configuration file used in SDT batch mode. You may alter this file to process a different range of orbits. Refer to the included files about SDT batch within the man-pages of SDT. Batch_processing of orbits 1-20000 have been completed. Orbits 5000-5549 have different file formats, resulting in one less data column (B_MODEL_GEO). There is not conflict with the MATLAB side as we read in the B_MODEL_GEI and do transformations to get the GEO form.

Log for errors that occur while running batch mode are contained in the following files in the same directory that issued SDT:

errUI

errdqh

errfast

errscm

outUI

outdqh

outfast

outscm

Files that display information for the IDL error are (for Llama):

```
outIDL.batch_go.pro
```

```
errIDL.batch_go.pro
```

For VIPER and ISR:

```
outIDL.batch_go.pro
```

```
errIDL.batch_go.pro
```

```
outIDL.timeout_go.pro
```

```
errIDL.timeout_go.pro
```

Access to SDT is limited to a single server, therefore one copy running on a machine at a given time.

Due to conflicts with VIPER and ISR not being able to issue an SQL query to the fast DB, the coding for obtaining the current orbit number while in batch mode is a bit different. It grabs the orbit data from `get_fa_orbit`, rather than using `what_orbit_is()`.

Llama is unaffected and can use `what_orbit_is()`. Speculation leads to Berkeley servers not being able to authenticate the server upon connection.

Below are listed files and folders of importance:

Llama:

```
username: nicole
```

```
password: *****
```

```
local config directory : /home/nicole/fast
```

```
location of sdt_test.batch : /home/nicole/sdt_test.batch
```

```
sdt directory : /home/nicole/software/sdt_releases/sdt
```

idl directory : /home/nicole/software/sdt_releases/sdt/idl
fast config directory : /disks/fast/software/config
processed data directory : /mnt/barracuda/sdt_releases/data
folder cleanup script : /home/nicole/folders.c
compile command : gcc folders.c -o folders, run with ./folders

VIPER:

username: schen
password: *****
local config directory : /mnt/barracuda1/schen
location of sdt_test.batch : /mnt/barracuda/schen/sdt_test.batch
sdt directory : /mnt/barracuda1/schen/fast/software/sdt
idl directory : /mnt/barracuda1/schen/fast/software/sdt/idl
fast config directory : /mnt/barracuda1/schen/fast/software/sdt/sdt_config
processed data directory : /mnt/barracuda1/schen/processeddata
folder cleanup script : /mnt/barracuda1/schen/folders.c
compile command : gcc folders.c -o folders, run with ./folders

ISR:

username: schen
password: *****
local config directory : /home/schen/
location of sdt_test.batch : /home/schen/sdt_test.batch
sdt directory : /home/schen/software/sdt/sdt_releases/sdt
idl directory : /home/schen/software/sdt/sdt_releases/sdt/idl
fast config directory : /home/schen/software/sdt/sdt_config
processed data directory : /home/schen/processeddata
folder cleanup script : /home/schen/folders.c

compile command : gcc folders.c -o folders, run with ./folders

IDL files that were modified (located in the idl directory):

make_efields_cdf.pro

make_all_cdf.pro

get_fa_attitude.pro

batch_processing.pro

batch_go.pro

*****Kinetic Energy Flux Information*****

The kinetic energy flux data is obtained independently of the Poynting flux data.

1. Open IDL on a windows machine.
2. You must have the "fast_software" and "ssl_berkeley" library folder installed. This can be obtained through asking me through E-mail or contacting Dr. James McFadden.
3. Then by creating a script with the IDL routine fa_k0_load you can download both the 'ies' and 'ees' data.

```
fa_k0_load,'ees',orbit=i, version = '04'
```

```
fa_k0_load,'ies',orbit=i, version = '04'
```

This will load orbit number 'i' and save that data to C:\Data by default.

4. Inclusion of such a script can be found within one of the workspaces on the SRI machine.

If there are any questions please do not hesitate to ask me at
googly.bear@gmail.com.

-Steven Chen

C.2 MATLAB Code

Please refer to the the MATLAB top level function `process_orbit.m` for a complete tutorial on how to run all necessary sub-functions.

Bibliography

- [1] R. Cosgrove and H. Bahcivan, "SRI Proposal EXU 09-001," National Science Foundation, Tech. Rep., 2009.
- [2] "Geomagnetic ap, Ap, Cp, and C9 Indices," retrieved: February 28, 2011. [Online]. Available: http://www-app3.gfz-potsdam.de/kp_index/apdescription.html
- [3] SRI International, "About Us," 2010, retrieved: November 13, 2010. [Online]. Available: <http://www.sri.com/about/>
- [4] "Ionosphere/Atmosphere - Sun Earth Plan," retrieved: November 13, 2010. [Online]. Available: <http://www.sunearthplan.net/5/ionosphere-atmosphere>
- [5] M. Rosenberg, "Layers of the Atmosphere," retrieved: November 22, 2010. [Online]. Available: <http://geography.about.com/od/physicalgeography/p/layeratmosphere.htm>
- [6] "Ionosphere and Magnetosphere (Atmospheric Science)," Retrieved: February 27, 2011. [Online]. Available: <http://www.britannica.com/EBchecked/topic/1369043/ionosphere-and-magnetosphere>
- [7] "Living With A Star: 6: Sun-earth Connection: Ionosphere," retrieved: February 18, 2011. [Online]. Available: http://ds9.ssl.berkeley.edu/lws_gems/6/secef_9.htm
- [8] T. Rosenvinge, "NASA's Cosmicopian - Sun - Earth's Magnetosphere," retrieved: November 21, 2010. [Online]. Available: <http://helios.gsfc.nasa.gov/magnet.html>
- [9] "Solar Wind," Retrieved: December 15, 2010. [Online]. Available: <http://www.britannica.com/EBchecked/topic/553057/solar-wind>
- [10] "Aurora (Atmospheric Phenomenon)," Retrieved: December 15, 2010. [Online]. Available: <http://www.britannica.com/EBchecked/topic/43410/aurora>

- [11] N. Otani, "Particle Simulations of Auroral Electron Acceleration," retrieved: March 8, 2011. [Online]. Available: http://otani.vet.cornell.edu/auroral_accel/index.html
- [12] "Space Weather," Retrieved: November 13, 2010. [Online]. Available: http://www.spaceweathercenter.org/SWOP/About_SW/Intro/1.html
- [13] R. Fischer, "National Space Weather Program," retrieved: November 22, 2010. [Online]. Available: http://www.nswp.gov/nswp_index.htm
- [14] "IMPACTS of Space Weather ," retrieved: February 28, 2011. [Online]. Available: http://solarb.msfc.nasa.gov/science/space_weather/
- [15] B. University of California, "Fast Auroral SnapshoT Explorer," retrieved: March 14, 2011. [Online]. Available: <http://sprg.ssl.berkeley.edu/fast/>
- [16] T. Quinn, "Fast Auroral SnapshoT Explorer," retrieved: November 13, 2010. [Online]. Available: <http://sprg.ssl.berkeley.edu/fast/scienceops/conus.php>
- [17] J. P. McFadden, R. Ergun, C. Carlson, W. Herrick, J. Loran, J. Verneti, W. Teitler, K. Bromund, and T. Quinn, "Science operations and data handling for the fast satellite," *Space Science Reviews*, vol. 98, pp. 169–196, 2001, 10.1023/A:1013179624253. [Online]. Available: <http://dx.doi.org/10.1023/A:1013179624253>
- [18] "CDF User's Guide," January 2011, Retrieved: February 27, 2011. [Online]. Available: <ftp://cdaweb.gsfc.nasa.gov/pub/cdf/doc/cdf33/cdf33ug.pdf>
- [19] "CDF Frequently Asked Questions," retrieved: February 5,2011, 2010. [Online]. Available: <http://nssdc.gsfc.nasa.gov/cdf/html/FAQ.html>
- [20] N. Cahill and S. Musielak, "Poynting Flux and Kinetic Energy Flux Derived from the FAST Satellite," Worcester Polytechnic Institute, Unpublished Major Qualifying Project, 2010. [Online]. Available: <http://www.wpi.edu/Pubs/E-project/Available/E-project-030810-151147/>
- [21] "Spin Axis- Right Ascension and Declination," retrieved: January 26,2011. [Online]. Available: <http://abyss.uoregon.edu/ js/ast221/lectures/lec03.html>

- [22] “11. Geographic Coordinate System,” retrieved: February 18, 2011. [Online]. Available: <https://www.e-education.psu.edu/natureofgeoinfo/book/export/html/1680>
- [23] A. Olsson, P. Janhunen, T. Karlsson, N. Ivchenko, and L. G. Blomberg, “Statistics of joule heating in the auroral zone and polar cap using astrid-2 satellite poynting flux,” Swedish Institute of Space Physics, Tech. Rep., 2004.
- [24] R. Thayer, *Ionospheric Electrodynamics: A Tutorial*. American Geophysical Union, 2000, Retrieved: November 22, 2010.
- [25] “Electromagnetic Energy,” retrieved: November 13, 2010. [Online]. Available: <http://www.phy.duke.edu/~lee/P54/energy.pdf>
- [26] “ONERA-DESP Library User’s Guide,” retrieved: February 27, 2011. [Online]. Available: http://craterre.onecert.fr/support/user_guide.html
- [27] “Magnetic Fields and Electricity,” retrieved: February 18, 2011. [Online]. Available: <http://library.thinkquest.org/C001429/electricity/electricity10.htm>
- [28] J. M. De Freitas, “POLAR3D: A 3-Dimensional Polar Plot Function in *Matlab*[®],” Version 1.2. QinetiQ Ltd, Winfrith Technology Centre, Winfrith, Dorchester DT2 8XJ. UK. 2 June 2005.
- [29] Y. Deng, A. Maute, A. D. Richmond, and R. R. G., “Analysis of thermospheric response to magnetospheric inputs,” *Journal of Geophysical Research*, vol. 113, 2008, 10.1029/2007JA012840. [Online]. Available: <http://dx.doi.org/10.1029/JA012840>